



# Slumping and mass transport deposition in the Nankai fore arc: Evidence from IODP drilling and 3-D reflection seismic data

## Michael Strasser

*MARUM-Centre for Marine Environmental Science, University of Bremen, D-28359 Bremen, Germany (mstrasser@uni-bremen.de)*

## Gregory F. Moore

*Department of Geology and Geophysics, University of Hawai'i at Mānoa, Honolulu, Hawaii 96822, USA (gmoore@hawaii.edu)*

## Gaku Kimura

*Department of Earth and Planetary Science, University of Tokyo, Tokyo 113-0033, Japan (gaku@eps.s.u-tokyo.ac.jp)*

## Achim J. Kopf

*MARUM-Centre for Marine Environmental Science, University of Bremen, D-28359 Bremen, Germany (akopf@uni-bremen.de)*

## Michael B. Underwood and Junhua Guo

*Department of Geological Sciences, University of Missouri, Columbia, Missouri 65211, USA (UnderwoodM@missouri.edu; jg2kc@mizzou.edu)*

## Elizabeth J. Screaton

*Department of Geology, University of Florida, Gainesville, Florida 32611, USA (screaton@ufl.edu)*

[1] Multiple lines of evidence exist for a range of sediment mass movement processes within the shallow megasplay fault zone (MSFZ) area and the adjacent slope basin in the outer fore arc of the Nankai subduction zone, Japan. Diagnostic features observed in three-dimensional reflection seismic data and in cores of the Integrated Ocean Drilling Program (IODP) document a multifarious mass movement history spanning ~2.87 million years. Various modes and scales of sediment remobilization can be related to the different morphotectonic settings in which they occurred. From this evidence, we decipher the tectonic control on slumping and mass transport deposition in the Nankai fore arc. Three periods of intensified mass wasting coincided with pulses of enhanced activity on the splay fault: (1) an initial phase of juvenile out-of-sequence thrusting ~1.95 to 1.7 Ma, (2) a reactivation phase between ~1.55 and 1.24 Ma, and (3) at about 1 Ma, during a phase of uplift of the fore-arc high and motion along the MSFZ. We suggest that slope oversteepening, extensional stress regimes, and lateral transmission of fluid overpressures may have preconditioned the slope sediments to fail. Individual mass-wasting events may have been triggered by dynamic loading from earthquake waves and/or transient pulses of pore pressure along the splay fault. Overall, our results provide insights into the complicated interplay between tectonic and submarine mass movement processes. We demonstrate that detailed knowledge about the spatial and temporal distribution of submarine mass movements can be integrated into a holistic reconstruction of tectonostratigraphic evolution of accretionary margins.

**Components:** 12,500 words, 14 figures, 1 table, 2 animations.

**Keywords:** Nankai Trough; submarine mass movements; submarine landslides; IODP; 3-D seismic; tectonostratigraphic evolution.

**Index Terms:** 3070 Marine Geology and Geophysics: Submarine landslides; 3060 Marine Geology and Geophysics: Subduction zone processes (1031, 3613, 8170, 8413); 3022 Marine Geology and Geophysics: Marine sediments: processes and transport.

**Received** 10 November 2010; **Revised** 10 March 2011; **Accepted** 15 March 2011; **Published** 11 May 2011.

Strasser, M., G. F. Moore, G. Kimura, A. J. Kopf, M. B. Underwood, J. Guo, and E. J. Screaton (2011), Slumping and mass transport deposition in the Nankai fore arc: Evidence from IODP drilling and 3-D reflection seismic data, *Geochem. Geophys. Geosyst.*, 12, Q0AD13, doi:10.1029/2010GC003431.

**Theme:** Mechanics, Deformation, and Hydrologic Processes at Subduction Complexes,  
With Emphasis on the Nankai Trough Seismogenic Zone Experiment  
(NanTroSEIZE) Drilling Transect

**Guest Editors:** D. Saffer, H. Tobin, P. Henry, and F. Chester

## 1. Introduction

[2] Submarine mass movements are leading agents in downslope sediment mass transfer, sediment distribution, and shaping of seafloor topography. They are common on passive and active continental margins and play a major role in the stratigraphic evolution of sedimentary basin and continental slope environments [e.g., Hampton *et al.*, 1996; Locat and Lee, 2002; Lee *et al.*, 2007]. With attention increasingly focused on oceanic geohazards [e.g., Morgan *et al.*, 2008], submarine mass movements are gaining scrutiny because of their catastrophic impacts on both offshore infrastructures (pipelines, cables and platforms) and coastal areas (e.g., slide-induced tsunamis) [e.g., Masson *et al.*, 2006; Mosher *et al.*, 2010; and references therein]. Many studies have suggested that earthquake shaking is a likely ultimate trigger for initiation of slope failures [e.g., Keefer, 1984; Hampton *et al.*, 1996]. However, long-term causal factors, including tectonic oversteepening, climatic and oceanographic conditions controlling sea level, sedimentation patterns and gas hydrate stability, as well as margin hydrogeology and fluid flow regimes, exert key roles in preconditioning submarine slopes to fail (see review papers by Hampton *et al.* [1996], Locat and Lee [2002], Masson *et al.* [2006], Lee *et al.* [2007], and also Camerlenghi *et al.* [2007], Morgan *et al.* [2008], and references therein).

[3] Whereas most of the largest known failures occur on passive margins and volcanic slopes [e.g., Moore *et al.*, 1994; Hühnerbach and Masson, 2004; Chaytor *et al.*, 2009], submarine accretionary

wedges generally are loci of rather diffuse slope instability, with a high concentration of small- to medium-scaled slump scars and associated mass transport deposits (MTDs) [e.g., McAdoo *et al.*, 2004; Mosher *et al.*, 2008; Moore *et al.*, 2009]. Megaslides can also occur in subduction zones, however, due to steepening of the continental slope above underthrust relief (i.e., seamounts) on the subducting plate [e.g., von Huene *et al.*, 2004; Hühnerbach *et al.*, 2005; von Huene, 2008] and in the hanging wall block of thrust faults [e.g., Cochonat *et al.*, 2002; Yamada *et al.*, 2010]. The largest events may even affect the full width of the accretionary prism [Moore *et al.*, 1976; Goldfinger *et al.*, 2000]. Prodigious MTDs of this type have also been identified in outcrops on land, where they are often referred to as olistostromes [e.g., Lucente and Pini, 2008; Burg *et al.*, 2008]. These outcrop studies, paired with numerical and analog modeling, also document the influence of rapid mass redistribution on thrust wedge mechanics and, in turn, on the structural evolution of the margin [e.g., Camerlenghi and Pini, 2009; Smit *et al.*, 2010; Yamada *et al.*, 2010].

[4] Along the Nankai margin, which is the focus of this paper, many products of submarine mass movements have been identified in geophysical or core data [Ashi and Taira, 1992; Cochonat *et al.*, 2002; Henry *et al.*, 2002; Underwood *et al.*, 2003b; Martin *et al.*, 2004; McAdoo *et al.*, 2004; Moore *et al.*, 2007, 2009; Kinoshita *et al.*, 2009; Kawamura *et al.*, 2009, 2010; Strasser *et al.*, 2009; Kimura *et al.*, 2011]. In this study, we investigate multiple lines of evidence for slope failure at var-

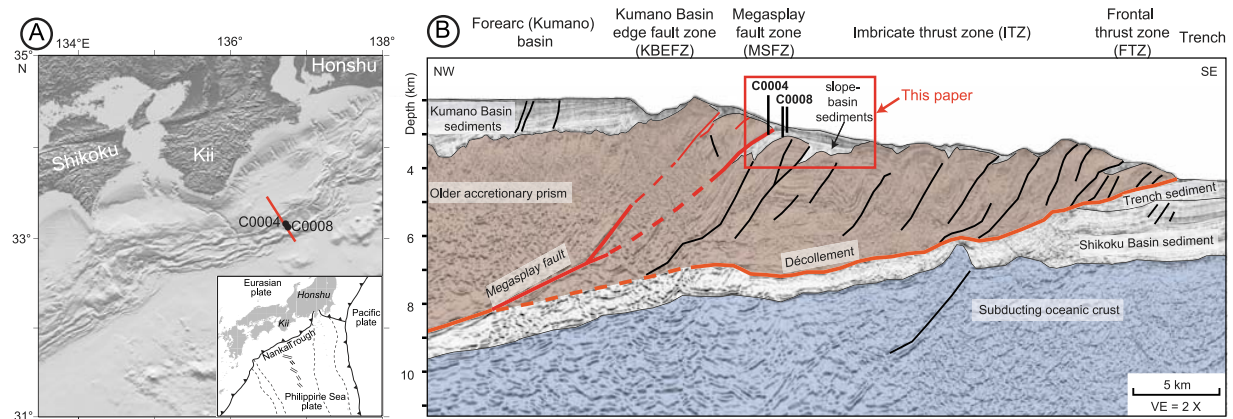


**Figure 1.** Geological setting of the Nankai accretionary wedge. (a) Shaded relief map of the Nankai Trough showing the regional setting of the IODP NanTroSEIZE drilling transect. The red line through IODP drill sites C0004 and C0008 shows the location of the seismic line cross section in Figure 1b. The inset is a tectonic map of the northern Philippine Sea plate. (b) Interpreted composite seismic line of the NanTroSEIZE transect showing the predominant morphotectonic zones. Figure 1 was modified from Moore *et al.* [2009]. VE, 2X (twofold vertical exaggeration).

ious scales, including (1) scars and MTDs in three-dimensional (3-D) reflection seismic data and (2) erosional surfaces and chaotic deposits in cores drilled during Integrated Ocean Drilling Program (IODP) Expedition 316 [Kimura *et al.*, 2008; Expedition 316 Scientists, 2009b, 2009c, 2009d], which are both part of the Nankai Trough Seismogenic Zone Experiment (NanTroSEIZE) [Tobin and Kinoshita, 2006]. By documenting slumping and mass transport deposition over a time span of more than 2 million years and by discussing their relation to the tectonostratigraphic evolution of the Nankai fore arc, we aim at identifying the different generic scenarios relevant for accretionary prism settings. Eventually, knowledge about the spatial and temporal distribution of submarine mass movements, along with a better understanding of their underlying geological processes aims at providing new insights on the tectonostratigraphic evolution of accretionary wedges.

## 2. Geological Setting

### 2.1. Nankai Accretionary Prism Along the Kumano Transect

[5] The Nankai accretionary complex off the coast of SW Japan is formed by subduction of the Philippine Sea plate beneath the Eurasian plate along the Nankai Trough (Figure 1a). The SW-NE striking accretionary wedge mainly consists of scraped-off and underplated strata from the incoming trench fill and Shikoku Basin. This study focuses on the Kumano transect (Figure 1), which is divided (from

SE to NW) into six main morphotectonic zones: trench, frontal thrust zone (FTZ), imbricate thrust zone (ITZ), megasplay fault zone (MSFZ), Kumano Basin edge fault zone (KBEFZ), and the fore-arc (Kumano) basin [Moore *et al.*, 2009].

[6] In the trench zone, a thick wedge of Quaternary trench deposits overlies Miocene-Pliocene Shikoku Basin sediments and subducting igneous basement (Figure 1b). As is typical of other parts of the Nankai Trough, there is a well-developed proto-thrust zone (PTZ), but the PTZ is overlain by a slice of trench strata previously accreted into the prism and emplaced over the trench strata by an out-of-sequence thrust (OOST) [Moore *et al.*, 2009; Sreaton *et al.*, 2009]. The FTZ, therefore, is highly complex with steep slopes and a large embayment interpreted as a slump scar, possibly reflecting indentation by a recently subducted seamount [Moore *et al.*, 2009]. The deposits from this prism toe collapse are found as irregular hummocky bathymetry seaward of the embayment, and the trench axial channel has been deflected significantly due to axial flows moving around the obstruction [Moore *et al.*, 2009; Kawamura *et al.*, 2010].

[7] Landward of the deformation front is the ITZ, a series of thrust packages reflecting past in-sequence thrusting and accretion. The ITZ is overlain by slope sediments deposited in slope basins within the ridge basin topography typical of fold-and-thrust belts developed in many accretionary prisms [e.g., Morley, 2009]. The slope basins and their deposits generally increase in depth and thickness landward from southeast to northwest (Figure 1b).

[8] Beneath the upper slope and Kumano Basin, a regional splay fault system, first recognized by *Park et al.* [2002] and later termed “megaspaly” by *Tobin and Kinoshita* [2006], discontinuously cuts across the older part of the accretionary prism [*Moore et al.*, 2007, 2009]. The shallow part of the MSFZ is a complex thrust system with backward breaking branches that truncate the imbricate thrust faults within the accretionary prism and override younger slope basin sediments [*Moore et al.*, 2007] (see section 2.2 below). Landward of the MSFZ, along the fore-arc high, the Kumano fore-arc basin is bordered on the southeast by a topographic valley. Beneath the valley is a fault zone that may have a combination of normal and strike-slip faults (KBEFZ [*Martin et al.*, 2010]). More than 1 km of sediment is imaged in the Kumano fore-arc basin. The seaward portion of the basin section is progressively tilted toward land, likely because of repeated motion on the megaspaly fault [*Park et al.*, 2002]. New analyses of data by *Gulick et al.* [2010] point toward a major phase of landward tilting and inferred megaspaly activity between 1.3 and 1 Ma. This activity postdates an earlier phase of asymmetric fore-arc high uplift (strongest uplift in the southwestern part of the Kumano transect) that may have occurred in concert with splay fault steepening and underthrusting of a large volume of sediment beneath the thrust [*Bangs et al.*, 2009].

## 2.2. Shallow Megaspaly Fault Zone and Adjacent Slope Basin

[9] Our study focuses on the shallow MSFZ area and an adjacent slope basin that is being overridden by the accretionary prism in the hanging wall. Previous studies indicated that the tectonostratigraphic system in this area started ~2.2 Ma in a frontal prism toe position when an emerging trench slope basin was formed in concert with in-sequence forward imbrication of accreted strata [*Strasser et al.*, 2009]. Splay fault movement initiated ~1.95 Ma as an OOST in the lower part of the prism. Since ~1.55 Ma, this initial OOST was uplifted and became reactivated, favoring ongoing “megaspaly” slip along it [*Strasser et al.*, 2009]. In the eastern part of the study area, along the NanTroSEIZE drilling transect, it appears that displacement along the shallow segment of the megaspaly fault ceased ~1.24 Ma, suggesting that it only experienced a relatively short period of high activity between ~1.55–1.24 Ma [*Strasser et al.*, 2009]. Along the seawardmost shallow megaspaly branch in the western part, there is no substantial movement recorded during that period, possibly due

to folding of the deeper splay fault in this area [*Kimura et al.*, 2011; *Bangs et al.*, 2009].

[10] After a short reactivation phase around 1.24 Ma, the seaward most branch in the western part of the study area became inactive [*Kimura et al.*, 2011]. However, seismic data clearly show that the megaspaly truncates very young sediments near the seabed west of the study area [*Moore et al.*, 2007], indicating that various small segments of the fault system are moving somewhat independently. As a result, slip along the splay fault in the study area might not be in the shallow branch but in other branches located landward [*Moore et al.*, 2007]. Furthermore, structural interpretation of 3-D seismic data by *Kimura et al.* [2011] demonstrates that the deformation is not limited to the splay fault, itself, but results in much broader and scattered deformation. Thus, splay fault activity and deformation in the surrounding geologic bodies are interrelated. This linkage is evident from ENE striking elongated anticlines that repeatedly developed in the accretionary prism underlying the slope basin seaward of the MSFZ; the anticlines resulted in synsedimentary doming of the slope sediments, development of NW and WNW trending normal faults, and frequent mass wasting [*Kimura et al.*, 2011]. The northern wing of one prominent anticline has a gentler dip than the southern limb, resulting in an asymmetric separation of the slope basin into two parts: an upper, up to 600 m thick basin that deepens toward NW, where it is overridden by the splay fault, and a lower, up to 1000 m thick basin that deepens toward SW (Figure 2). The transition from the upper to the lower basin correlates to a seaward dipping low-angle on-lap surface (inferred unconformity) and a bathymetric step along which several slump scars occur (Figure 2). Numerous small-scale slump scars are also present in the hanging wall block of the splay fault, in particular in the western part, where the slope is generally rougher and steeper (Figure 2) [*Kimura et al.*, 2011].

## 2.3. Lithostratigraphy and Seismic Stratigraphy of the Upper Slope Basin

[11] IODP NanTroSEIZE Stage 1 drilled three locations in this area (multiple holes at Site C0004, Hole C0008A, and Hole C0008C) (Figures 1–3). The results from Holes C0008A and C provide a reference section of sediments in the upper slope basin. Site C0004 cored the accretionary prism in the hanging wall of the splay fault, slope sediments that lie above the prism, and slope basin sediments

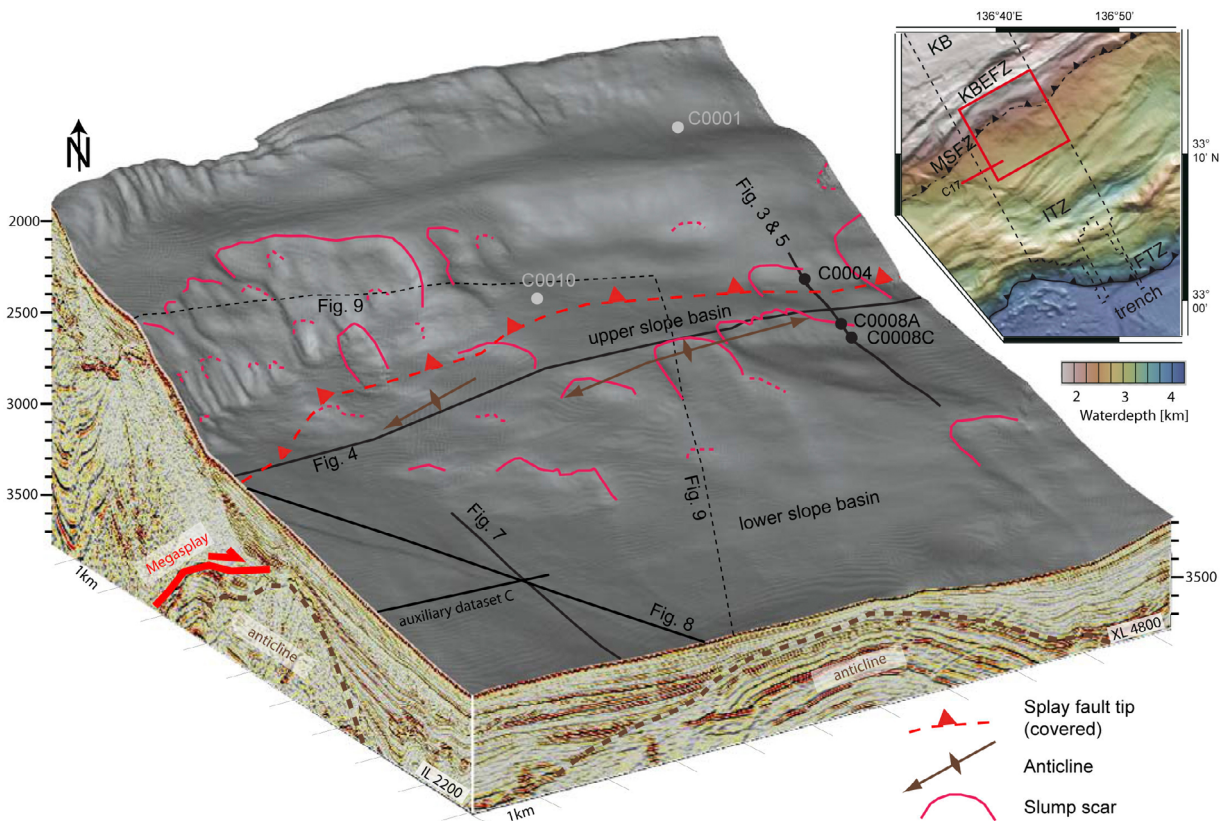


**Figure 2.** Perspective view of 3-D seismic volume and overlain bathymetry of the study area showing the prominent structural elements (i.e., shallow, seawardmost branch of the MSFZ and anticline structures within the underlying accretionary prism), surface expression of recent slope failures, location of NanTroSEIZE drill sites, seismic lines (solid black lines; shown in Figures 3–5, 7, and 8), and outline of maps (dashed black lines; shown in Figure 9). The map in the upper right corner is modified from Moore *et al.* [2009] and shows the location of the study area (red square represents outline of perspective 3-D block) with respect to the predominant morphotectonic zones (see Figure 1 for abbreviation), outline of 3-D seismic box (dashed box), and location of CDEX 2-D seismic line (C17) [Taira *et al.*, 2005] shown in Figure S3 in the auxiliary material.

that are in the footwall of the splay fault. Figure 3 and Table 1 summarize the compiled lithostratigraphy and age constraints for key stratigraphic horizons and sedimentary units used in this study. At Hole C0008A, the slope basin stratigraphic succession unconformably overlies the older accretionary prism composed of sand-rich trench wedge turbidites. Collectively, these units now form the top of the anticlinal structure and comprise (from bottom to top) the following.

[12] Unit 1c, which is dominated by greenish-gray silty clay with beds of sand, sandy silt, silt, and volcanic ash layers. The lowermost part of this unit consists of a 40 m thick succession comprising MTDs that were deposited between ~1.95 and 1.65–1.8 Ma ([*Expedition 316 Scientists*, 2009d] see details below in section 4.2). In the middle part of Unit 1c, a key seismic horizon of high reflectivity

can be correlated throughout the upper slope basin (seismic horizon A) and matches a coarse ~3.5 m thick sand layer in the core.

[13] Unit 1b, which consists of several parallel high-reflective horizons within the middle of the slope basin that correlate to a stratigraphic succession showing abundant coarse turbidite layers interbedded with greenish-gray silty clay and volcanic ash. Nannofossils and magnetostratigraphy document that unit 1b ranges from ~1.55 Ma to 1.07 Ma in age [*Expedition 316 Scientists*, 2009d].

[14] Unit 1a, which is the uppermost unit of slope sediments. It is composed mainly of greenish-gray silty clay and silt turbidites with several ash layers. Nannofossils and magnetostratigraphy document a significant hiatus (extending from ~0.9 Ma to 0.06 Ma) near the top of the stratigraphic succession (see details below in section 4.2).

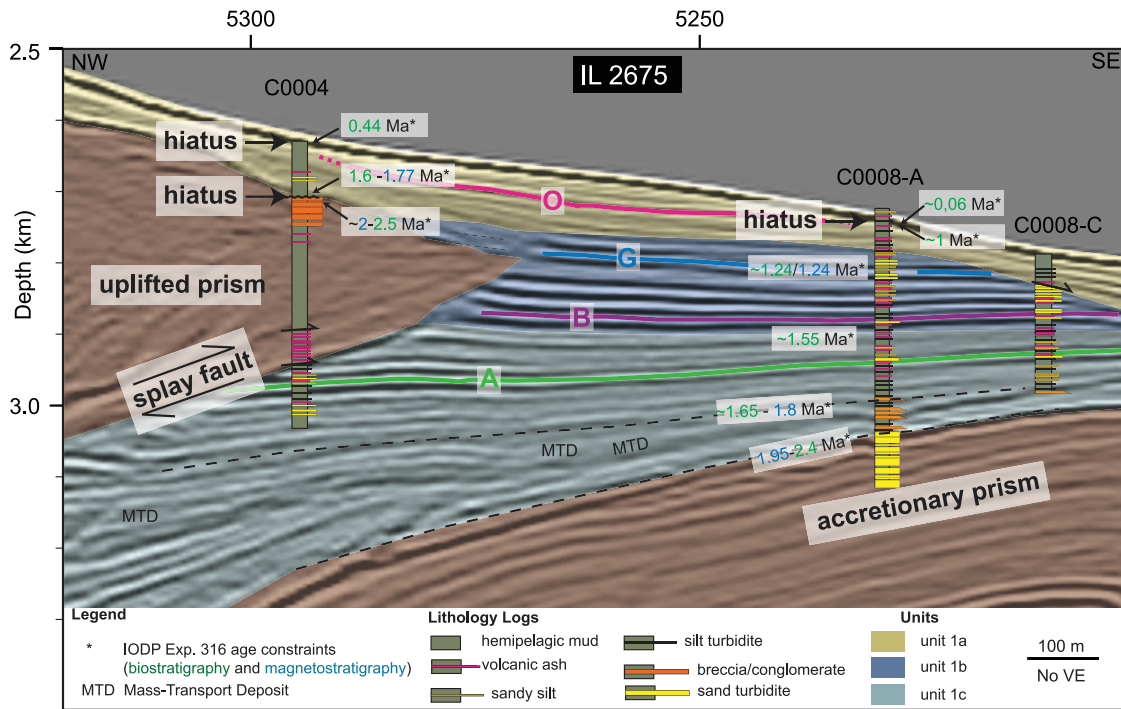


**Figure 3.** Data compilation across the shallow megasplay system: detail and interpretation of seismic inline IL 2675 crossing IODP Sites C0004, C0008A, and C0008C. The location is shown in Figure 2. The horizontal axis indicates crossline numbers. Overlain are lithostratigraphic sections of drill sites and age constraints after *Expedition 316 Scientists* [2009c, 2009d], and the units are defined by *Kimura et al.* [2011]. A, B, G, and O indicate key seismic stratigraphic horizons followed in Figures 3–5, 7 and 8.

[15] At Site C0004, slope sediments above the uplifted accretionary prism are composed of greenish-gray silty clay, silty and sandy turbidites, and several ash layers. Their ages range from ~1.7 Ma at the base to Holocene at the seafloor (Figure 3). As pointed out by *Kimura et al.* [2011], the stratigraphic succession is not temporally continuous and is affected by erosion. As a result, comparable unit subdivisions and detailed correlation with slope sediments at Site C0008 are impossible. This interpretation of missing section is supported further by the occurrence of a biostratigraphic datum equal to 0.44 Ma at a depth of only 8.4 m below seafloor (mbsf) (X. Su, Data report: Occurrence of age-diagnostic nannofossil species and biostratigraphic datum at IODP Exp. 316 Sites C0004 and C0008, Nankai Trough, submitted to *NanTroSEIZE Stage 1: Investigations of Seismogenesis, Nankai Trough, Japan, Proceedings of the Integrated Ocean Drilling Program, 314/315/316*, 2010; see details below in section 4.2).

[16] At the base of the slope sediments that lie above the uplifted prism, there is a sharp angular unconformity with a hiatus spanning ~200 to 500 kyr [Expedition 316 Scientists, 2009c] (Figure 3),

below which a 30 m thick interval of sedimentary breccias was recovered in Hole C0004C. Nearby drilling at Hole C0004D (at ~30 m distance) did not record any evidence for sedimentary breccias in the correlative depth-age interval ([Expedition 316 Scientists, 2009c] see details below in section 4.2).

[17] Sediments overridden by the splay fault at Site C0004 consist of dark olive gray silty clay with common thin sand and silt beds. These sediments

**Table 1.** Summary of Dating Stratigraphic Units and Key Horizons Used in This Study<sup>a</sup>

Stratigraphic Units	Age Range
Unit 1a	1.07 Ma–present
Unit 1b	1.55–1.07 Ma
Unit 1c	1.95–1.55 Ma
Seismic Horizons	Mean Age
Horizon A	1.7 Ma
Horizon B	1.5 Ma
Horizon G	1.3 Ma
Horizon O	1.0 Ma

<sup>a</sup>Table 1 integrates previous work by *Expedition 316 Scientists* [2009d], *Strasser et al.* [2009], *Kimura et al.* [2011], and Su (submitted manuscript, 2010). Ages are rounded mean values of ranges for maximum and minimum ages (see details in Figures S1 and S2).

can be correlated on the basis of both age and lithology to the upper half of unit 1c recovered at Site C0008A (Figure 3). *Expedition 316 Scientists* [2009c, 2009d] reported significantly lower porosities in the underthrust section compared to the reference section at Site C0008, suggesting that permeability is sufficiently high to allow compaction following underthrusting [Kimura *et al.*, 2008].

### 3. Material and Methods

#### 3.1. 3-D Seismic Data

[18] Seismic data presented here are part of a 12 km wide, 60 km long, 3-D seismic reflection volume acquired using a commercial seismic vessel towing two air gun source arrays (each totaling 3090 cu in) and four 4.5 km long hydrophone streamers [Moore *et al.*, 2009]. The recorded seismic wavefield data were processed first using a 3-D prestack time migration, and later a prestack depth migration was performed (see details of processing procedures in the study by Moore *et al.* [2009]). The interval between inlines (oriented NW-SE) and crosslines (oriented SW-NE) of the resulting data set is 18.75 m and 12.5 m, respectively. The vertical resolution for the interval of interest in this study is between 5 and 20 m (i.e., 5–7 m near the seafloor, 10–20 m at depths near 1400 mbsf [Moore *et al.*, 2009]).

[19] In order to investigate the temporal and spatial distribution of the observed mass movement features in core and seismic data, and to study its relationship to the overall slope basin tectono-stratigraphic evolution and splay fault activity, we correlate age constraints from cores along the NanTroSEIZE drilling transect [Expedition 316 Scientists, 2009c, 2009d; Su, submitted manuscript, 2010] with the 3-D seismic data. Key horizons are mapped throughout the slope basin using standard seismic stratigraphic mapping tools implemented in the *Paradigm* seismic interpretation software. Details of seismic-to-core correlation, seismic stratigraphy and seismic-horizon correlation from the upper to the lower slope basin are presented in Figures S1 and S2 in the auxiliary material.<sup>1</sup>

#### 3.2. Core Material Analysis

[20] Some of the core data presented here were generated on board D/V *Chikyu* during IODP Expedition 316 using standard IODP methods and

procedures (see explanatory notes in the study by *Expedition 316 Scientists* [2009b]). These data include visual split-core description (VCD), biostratigraphy and magnetostratigraphy, physical property measurements, and scanning of whole round core segments by X-ray computed tomography (X-CT). The latter creates a 3-D image of the core and enables visualization of internal sediment structure missed by conventional VCD.

[21] Selected samples from MTDs were analyzed postexpedition in laboratories at the MARUM, University of Bremen (physical index properties and MTD clast texture and shape) and the University of Missouri (X-ray diffraction analysis (XRD) of the clay size fraction). These data provide the means to infer the source and formation mechanism of the observed MTDs. Semi-indurated mud clasts were subsampled manually by picking under the microscope. The subsamples were analyzed for their physical index properties following the standard procedure after Blum [1997]. Using a handheld high-precision gauge we measured thickness (short length), width (intermediate length) and length (longest length) of 72 individual clasts and calculated elongation and flatness ratio as the ratio of thickness to width and the ratio of width to length, respectively. Elements of clast texture (particle shape, sphericity and roundness) were analyzed following Drake [1970] and Pettijohn *et al.* [1972]. The clay mineral assemblages were assessed after separating the clay size fraction (<2  $\mu\text{m}$ ) according to the methods of Underwood *et al.* [2003a]. We express each relative mineral abundance as a weight percent of the clay size fraction (where smectite + illite + chlorite + kaolinite + quartz = 100%). The calculations are based on peak areas for basal reflections and a matrix of normalization factors, which were solved for comparable mixtures of mineral standards using singular value decomposition (SVD). Average errors associated with measurements of the standard mineral mixtures are 2.7% for smectite, 0.9% for illite, 1.8% for chlorite + kaolinite, and 1.2% for quartz.

### 4. Results

#### 4.1. Evidence for Slope Failure and MTDs in 3-D Seismic Data

[22] Slope failures and resultant MTDs are typically recognized in seismic data by reflection truncations, on-lap geometries and their characteristic chaotic-to-transparent acoustic facies, respectively, which remain preserved in the geological

<sup>1</sup>Auxiliary materials are available in the HTML. doi:10.1029/2010GC003431.

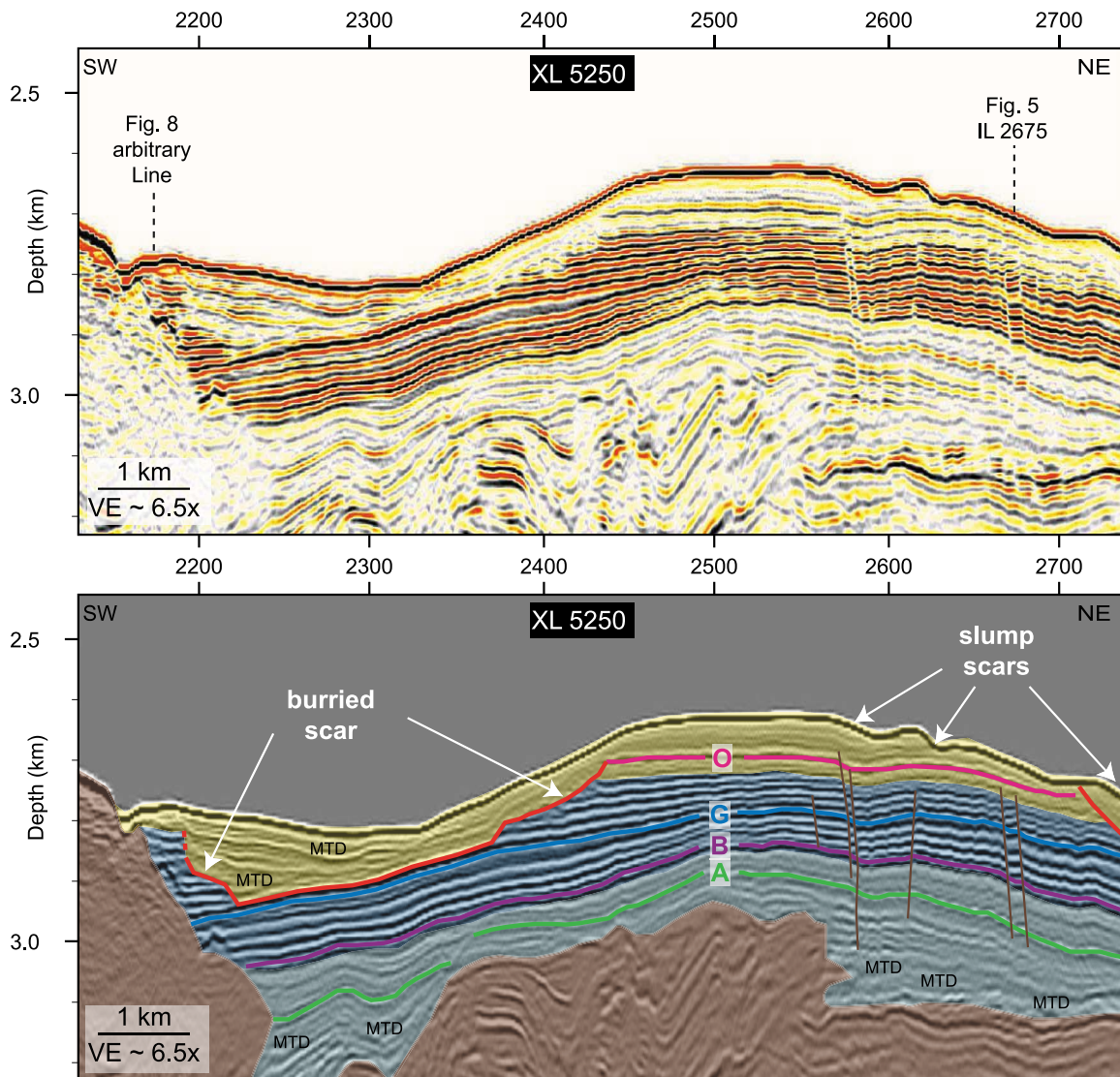


**Figure 4.** Seismic profile of (top) crossline 5250 and (bottom) its interpretation from the upper slope basin and along strike of the MSFZ. The location of the line is shown in Figure 2. The horizontal axis indicates inline numbers. The colors for interpretation and seismic stratigraphic horizons and units are the same as those in Figure 3. High-angle normal faults are indicated by brown lines. See text for detailed interpretation.

record long after their burial. Hence, seismic data contain characteristic fingerprints to identify and map products of submarine mass movement events throughout the slope basins.

[23] The succession of MTDs identified in cores from the lower slope basin deposits at Site C0008 (see section 2.3 above and more details in section 4.2 below) corresponds on seismic data to a package characterized by low-amplitude, fuzzy reflections with short lateral continuity (Figure 3). This body thickens toward the NW where it has been fully overridden by the hanging wall of the splay fault. Some individual MTDs are thick enough toward the NW to be seismically resolved (i.e., >10–20 m

in thickness), where they occur as wedge-shaped, low-amplitude bodies of a few hundred meters horizontal extent (Figure 3).

[24] Along strike, this MTD succession in the lower part of unit 1c can be followed in seismic data for several km, as evident in the slope-parallel seismic line shown in Figure 4. This observation suggests that early Pleistocene mass wasting occurred on a broader, regional scale. In contrast, the sedimentary breccias observed in the uppermost part of the prism at Site C0004C (see section 2.3 and more details below in section 4.2) have no obviously correlative acoustic facies that can be mapped spatially. They thus appear to be the product of a more localized

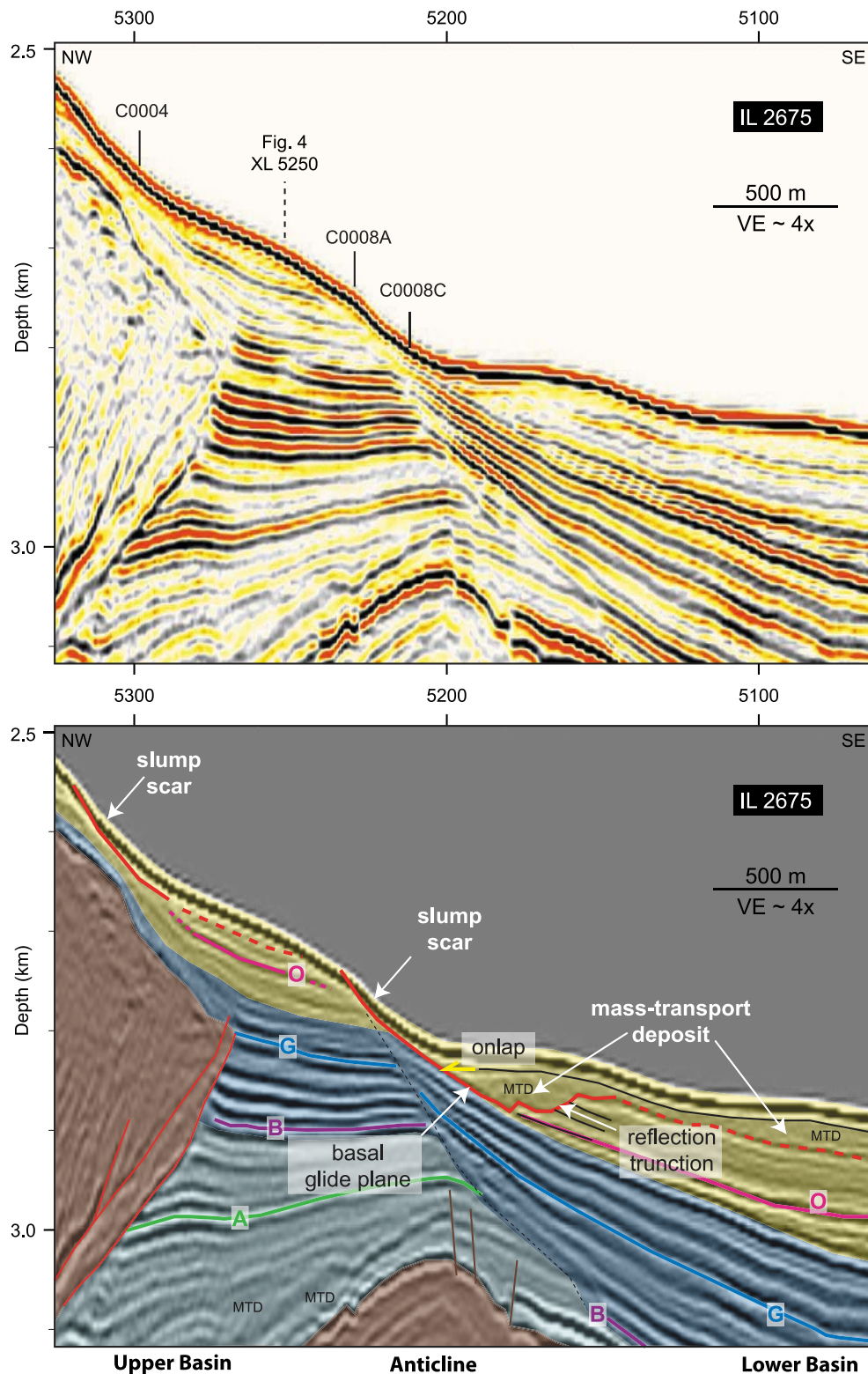


**Figure 5.** Seismic profile of (top) Inline 2675 and (bottom) its interpretation. The location of the line is shown in Figure 2. Figure 5 displays the same profile as in Figure 3, with higher vertical exaggeration and extended farther seaward (toward SE) to better illustrate the buried anticline structure (see Figure 2), and seaward dipping low-angle surface (see also *Kimura et al.* [2011] for more details) and products of submarine mass movements. The horizontal axis indicates crossline numbers. The colors for interpretation, seismic stratigraphic horizons and units are the same as those in Figures 3 and 4. See text for a detailed interpretation.

phenomenon, as also suggested by the absence of coeval sedimentary breccias in nearby Hole C0004D [*Expedition 316 Scientists*, 2009c].

[25] Geometric manifestations of the two age gaps in the shallow subsurface at Sites C0004 and C0008 (see section 2.3 and more details below in section 4.2) are expressed in bathymetric and seismic data. Figure 5, displaying the profile from Figure 3 with higher vertical exaggeration and extended seaward toward SE, shows two convex-downward erosional surfaces that truncate seismic reflections in the vicinity of Sites C0004 and C0008. Each of these surfaces correlates by depth to the stratigraphic hiatus observed in the cores, and their 3-D geometries relate to amphitheater-shaped slope failure scars in the bathymetry (Figure 2). The correlative shallow erosional features are also evident by reflection truncations in the eastern part of the along-strike profile shown in Figure 4. The maximum heights of the scars near Sites C0004 and C0008 are ~40 and 90 m, respectively. These values provide us with lower limits to the estimated thickness of material eroded from the relatively young submarine slope failure events.

[26] Southeast of Site C0008, a seaward dipping seismic reflection parallels the underlying reflection (Figure 5). We interpret this reflection as the basal glide plane of a rotational slide in the transition zone between the head scar and main deposition area of the associated MTD. This MTD is imaged in Figure 5 by an acoustically chaotic-to-transparent body up to 50 m thick and thinning toward SE. The youngest seismic reflection overlying the MTD laps onto the scar and the basal glide plane surface. In the proximal zone, the base of the MTD is defined by the seismic horizon correlative to the glide plane. Toward the distal edge of the basal glide plane, the base of the MTD successively steps upward, truncating successively younger horizons to the SE. The overall geometry is consistent with a rotational mode of mass movement, the defining attribute for slumps [e.g., *Lee et al.*, 2007, and references therein], with only minor translational slip along a layer-parallel glide plane in the transition zone and frontal ramping by the toe of the failed mass (Figure 6). Disintegration of strata during downslope transport likely evolved into a clast-and-matrix mass flow, leading to the distinctive chaotic-to-transparent acoustic facies of the MTD in the depositional area.

[27] As evident in Figures 2 and 5, slumping also results in a prominent bathymetric step at the location where the growing anticline structure se-

parates the upper and lower slope basin. There, NW and WNW trending normal faults are developed, and a seaward dipping low-angle surface cuts through the overlying slope sediments (Figures 3 and 5). The low-angle surface truncates seismic horizons of the upper slope basin; this truncation is particularly evident for the interval of parallel high-amplitude reflections of unit 1b. As also noted by *Kimura et al.* [2011], the low-angle surface appears to offset older stratigraphic horizons in a normal sense; however, in its shallower part it clearly coincides with the head scarp surface of the slump. Hence, the feature represents the slip zone of a slump onto which younger sediments onlap. In our conceptual slump model and resulting seismic geometries (Figure 6), onlap onto this unconformity may include “pseudo-onlaps” that form where strata drape the steeper slump scar and glide plane surface but become too thin to be seismically imaged (Figure 6c). This interpretation also explains the apparent offsets of seismic stratigraphic horizons as observed in Figure 5 (e.g., horizons G and B).

[28] Character and size of slumps in the shallow MSFZ area and along the seaward side of the growing anticline structure both vary along strike. Figure 4 shows that toward the west, the upper part of unit 1b displays prominent reflection truncations of horizons G to O (around inline (IL) 2450–2400 and 2200–2170); these truncations are indicative of a large mass-wasting event that eroded a ~5 km wide and up to 150 m thick slope portion in the SW part of the study area at a time coincident with the age of horizon O (estimated to be younger than 1.05 Ma but older than 0.9 Ma based on seismic-to-core correlation around Site C0008A, Table 1, Figure 3, and Figure S1). Its location also coincides with an area where the surface character of the steeper slope above the tip of the MSFZ changes from smooth and sediment covered, in the eastern part, to rough in the western part with many small-scale slumps scars that erode into the accretionary prism [*Kimura et al.*, 2011] (Figure 2). The depression excavated by this large mass-wasting event is still partly evident in the bathymetry (Figure 2), although it has been filled with up to 175 m of sediment. Within the postevent sedimentary succession, we see stacking of several small-scale, acoustically chaotic-to-transparent, wedge-shaped bodies (Figure 4). Those bodies are interpreted as MTDs resulting from repetitious slumping along the steep slope in the hanging wall block of MSFZ, as evidenced by many slump scars in Figure 2.

[29] The diagnostic fingerprints of MTDs, including (1) chaotic-to-transparent acoustic facies overlying

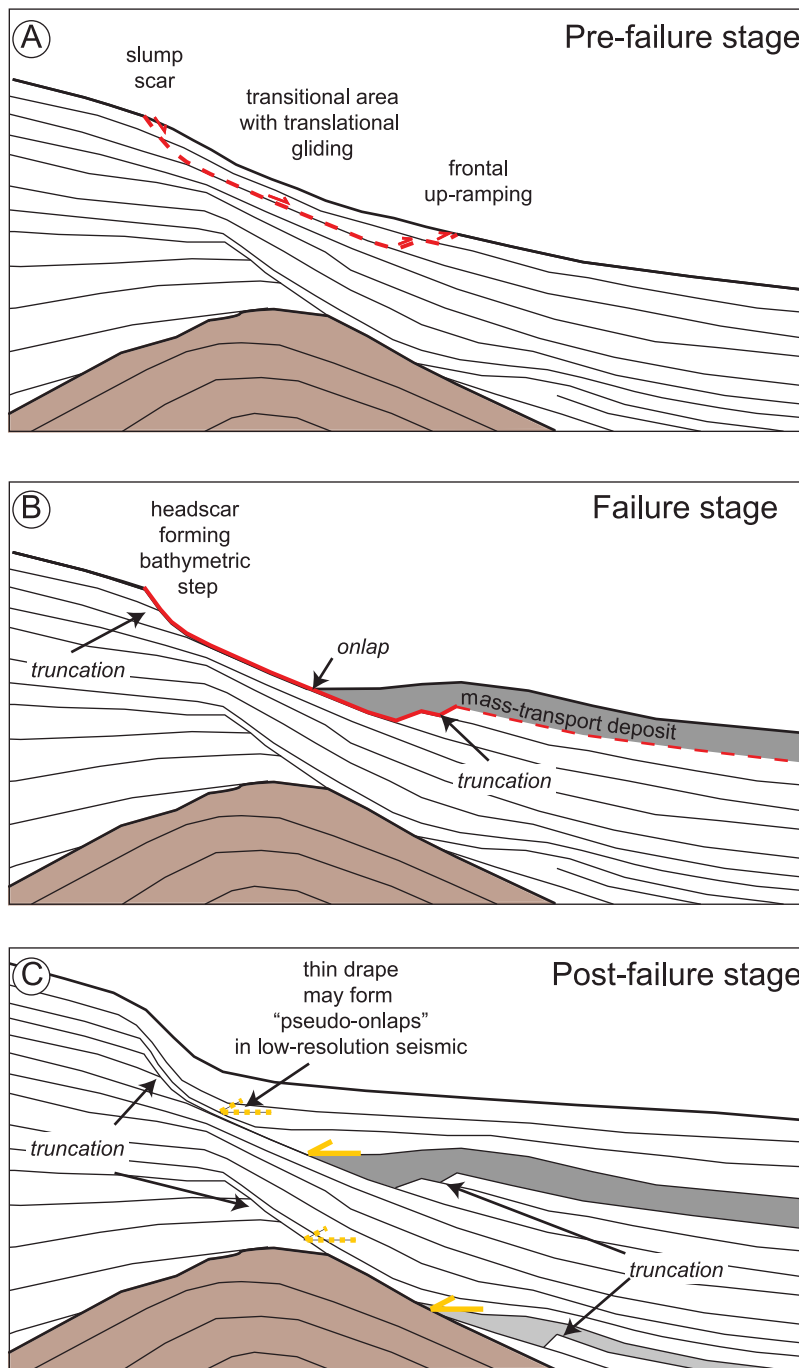


**Figure 6.** Schematic conceptual slump model and resulting geometries observed in seismic data reconstructed for (a) pre-failure stage, (b) failure stage, and (c) post-failure stage. The characteristic “slump fingerprint” in seismic data comprising chaotic-to-transparent acoustic facies, truncation, and on-lap geometries remain preserved in the geological record and thus allow for identifying and detail mapping of older slump events, as schematically shown in Figure 6c.

upramping reflection truncations and (2) on-lap geometries onto layer-parallel erosional surfaces, can be found throughout the lower slope basin, and they typically occur within the upper stratigraphic succession correlative to unit 1a. Figure 7 shows examples of buried MTDs and slump structures

along IL 2315. Here, as well as in the profile shown in Figure 8, the sedimentary succession of the lower slope basin shows distinct differences between unit 1a and 1b.

[30] Unit 1a is characterized by a low-amplitude reflection pattern and comprises laterally confined,

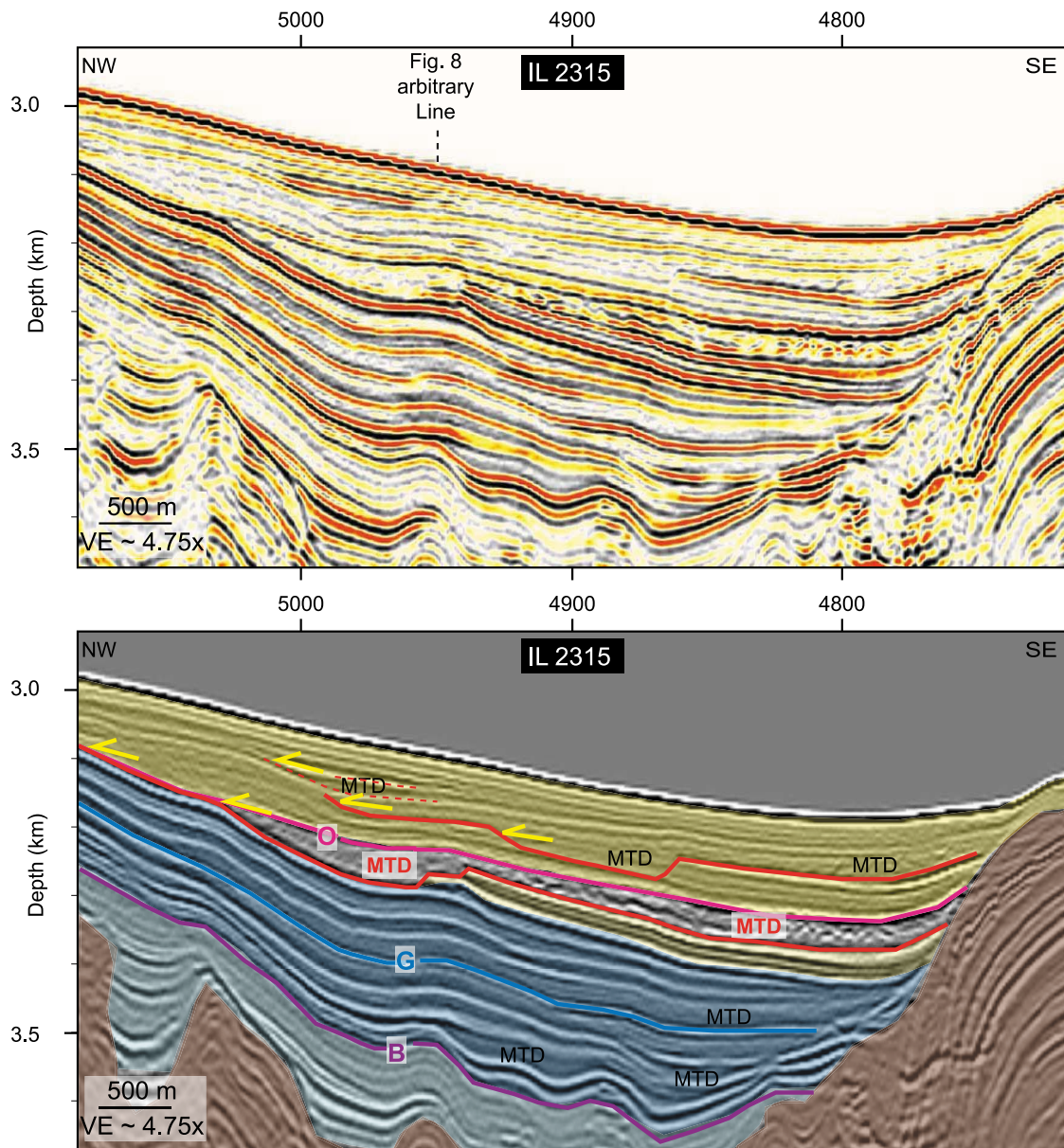


**Figure 7.** Seismic profile of (top) Inline 2315 and (bottom) its interpretation showing multiple-stacked slump features, MTDs, and the general stratigraphic succession of the lower slope basin. The location of the line is shown in Figure 2. The horizontal axis indicates crossline numbers. The colors for interpretation and seismic stratigraphic horizons and units are the same as those in Figures 3 and 4. See text for a detailed interpretation.

acoustically transparent-to-chaotic MTDs with several reflection truncations. The sedimentary regime is dominated by small- to medium-scale mass-wasting processes. Where slump fingerprints are identified in the shallower subsurface toward the east of IL 2315, they generally relate to slump scars along the topographic step above the anticline.

[31] Unit 1b comprises two types of acoustic facies: subparallel high-amplitude reflections, and low-amplitude wedges and layers that thin out toward

the basin flanks. We interpret the latter type of acoustic response as MTDs ranging from 20 m to 50 m in thickness and with substantial lateral extension, as they can be traced over several km along strike in 3-D seismic data (generally thickening toward SW, i.e., toward the depocenter of the lower slope basin). Alternatively, considering that the correlative interval of unit 1b at Site C0008 corresponds to interbedded thin turbidites and mud, the acoustic character and considerably higher thickness of unit 1b in the lower slope basin

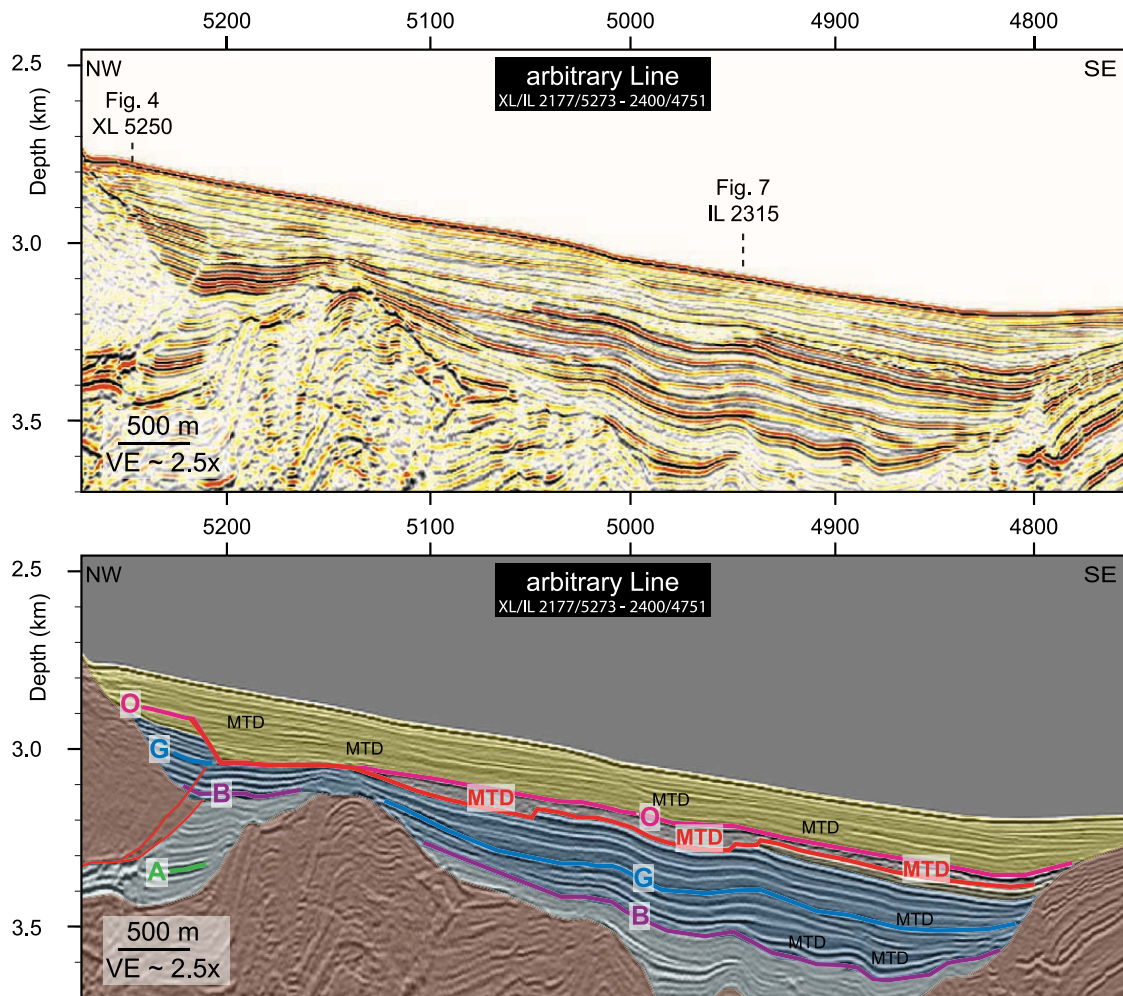


**Figure 8.** Seismic profile of an arbitrary line computed from (top) the 3-D seismic volume and (bottom) its interpretation showing a transect across the westernmost part of the large erosional area associated to time horizon O and across the proximal area of its related MTD, along with the general stratigraphic succession of the southwestern part of the upper basin and the lower slope basin. The location of the line is shown in Figure 2. The horizontal axis indicates crossline numbers. The colors for interpretation and seismo stratigraphic horizons are the same as those in Figures 3 and 4. See text for detailed interpretation.

may have resulted from turbidite deposition also focusing in the depocenter of the lower slope basin.

[32] A prominent MTD, associated to time horizon O and thus time correlative to the large erosional event described above, occurs at the transition between the two units and can be mapped over 20 km<sup>2</sup> (Figure 9). The MTD reaches a maximum thickness of 182 m in the SW corner of the 3-D seismic box, and it thins out ~2 km southwest of the area covered by the 3-D seismic cube, as imaged on a NE-SW trending seismic profile from the 2003 CDEX commercial 2-D survey (Figure S3) [Taira *et al.*, 2005]. We estimate the total volume of the MTD to be ~2 km<sup>3</sup>. This is based on 1.54 km<sup>3</sup> calculated from the 3-D seismic data plus ~0.5 km<sup>3</sup>

to account for additional volume outside of the 3-D seismic data, which is roughly 25% of the total MTD volume as indicated by 2-D seismic lines east of the 3-D box (Figure S3) [Taira *et al.*, 2005]. The base of the MTD comprises two steps, up to ~25 m and 45 m high (a shallower one in the northernmost part of the depositional area and a deeper one striking NE to SW in the middle-to-eastern part, respectively), that are characterized by upramping reflection truncation (Figures 7 and 8). These steps indicate that the mass movement eroded part of the lower basin's sedimentary succession within its area of deposition. Spatial mapping of these steps reveals that the deepest erosion took place in a scoop-shaped area in the shallowest, most proximal northern portion of the MTD (Figure 9). Mass

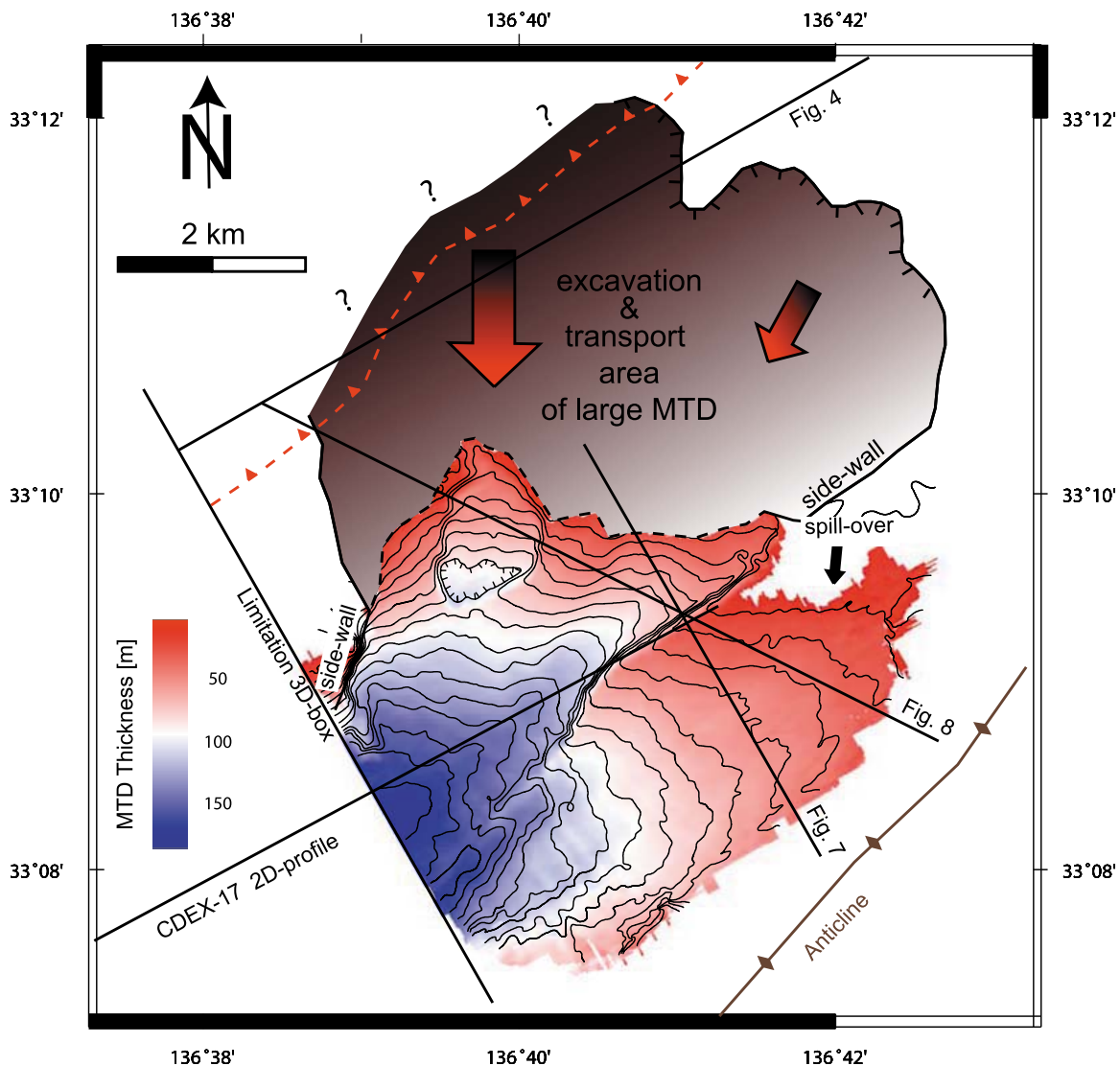


**Figure 9.** Iopach map (thickness) and interpreted excavation and transport area of large MTD associated to time horizon O (dated to ~1 Ma). The location of the map is shown in Figure 2. The isopach map is produced using horizon O (i.e., horizon immediately overlying the MTD) and the horizon mapping the interpreted base of the MTD (corresponding to red lines shown in Figures 7 and 8). The contour interval is 10 m. The excavation and transport area is derived from mapping reflection truncations (as shown exemplarily on Figures 4 and 8) and the locations where horizon O unconformably overlies older strata. The interpreted sidewall and spillover result from geometrical relationships of the inferred transport direction from NNE to SW. The red dashed line shows the projected tip at depth of the shallow seaward most branch of the MSFZ covered below slope sediments. See text for a detailed description and interpretation. Also shown are locations of seismic lines in Figures 4, 7, and 8 and of seismic line CDEX-17 shown in Figure S3.

movement from the north is consistent with the large, buried scar in the SW part of the upper slope basin (see above) being genetically related to the large MTD in the lower slope basin. This interpretation is reinforced by the correlation of reconstructed spatial geometries for head scars and sidewalls, as well as upramping structures and thickness distribution in the source and depositional area (Figure 9). The northwestern upslope extension

of the head scar cannot be constrained from 3-D seismic data, because it has been affected by continuous erosion of the accretionary prism by recent slumping along the steep slope in the hanging wall block of the MSFZ.

[33] Only in the westernmost portion, as imaged in the seismic line shown in Figure 8, does a possible relationship exist between the splay fault and slope

failure scar. The seaward most branch that accommodated most of the out-of-sequence displacement appears to have become inactive about 1.5 Ma (i.e., time equivalent to the deposition of seismic horizon B in Figure 8). Conversely, a younger and shallower, more landward branch of the splay fault cuts through into overlying slope sediments, thereby documenting short-term splay fault reactivation about 1.24–1 Ma [Kimura *et al.*, 2011]. Figure 8 shows that the tip of this young branch soles into the basal area of the slide scar. Thus, we suggest a possible cause and effect between splay fault activity and the initiation of large-scale slope collapse (see discussion in section 5.3 below).

#### 4.2. Evidence for Mass Movements in Core Along the NanTroSEIZE Drilling Transect

[34] Cores containing the oldest MTDs from the study area occur within the uppermost part of the accretionary prism in Hole C0004C, from a depth interval of 78.06–117.72 mbsf. The dominant lithology of this ~40 m thick, 2.06–2.87 Ma MTD succession is a synsedimentary breccia made of subangular clasts of pebble size with subsidiary silty clay horizons (hereafter termed upper Pliocene MTD). This interval was recognized only in Hole C0004C, as interpretation of the correlative depth interval at nearby Hole C0004D was hampered by low recovery and poor core quality [Expedition 316 Scientists, 2009c]. Both the clasts and the matrix of the breccia are composed of dark greenish gray silty clay without discernible compositional differences. The breccia is clast supported in places and matrix supported in others. Between them, homogenous muddy interbeds are found and interpreted to result from hemipelagic settling between episodic mass-wasting events. Patches of hemipelagic mud clasts occur near the base of breccia beds, indicating reworking of seafloor during mass-wasting deposition.

[35] The boundary between this upper Pliocene MTD and the overlying Pleistocene hemipelagic slope sediments is a sharp angular unconformity that dips ~50° (Figures 10a and 10b). The unconformity coincides with a significant hiatus spanning between 1.46 and 1.6 and 2.06–2.52 Ma, and between 1.77 and 1.95 Ma, as constrained by nannofossil biostratigraphy and magnetostratigraphy, respectively [Expedition 316 Scientists, 2009c; Su, submitted manuscript, 2010]. Bulk density increases down the borehole across the boundary from 1.68 to 1.79 g/cm<sup>3</sup>, and porosity abruptly decreases from ~59% to 53% [Expedition

316 Scientists, 2009c], consistent with the transition from less compacted Quaternary slope sediments to more compacted Pliocene prism sediments. Pyrite mineralization is clearly visible in the first 5 cm below the unconformity, where it forms cubes and aggregates of cubes that fill near-vertical fractures within the sedimentary breccias (Figure 10b and Animation S1). The pyrite-filled fractures end abruptly at the upper surface of the unconformity. From these observations, we suggest that strata immediately below the unconformity preserve a complicated paragenetic sequence that encompasses burial, chemical alteration, erosion, and perhaps prolonged seafloor exposure. In conjunction with the seismic data we interpret the angular unconformity to represent a fossil slide scar along which slope failure event(s) excavated part of the upper accretionary prism and slope apron, followed by burial beneath younger slope sediments.

[36] A series of interbedded mud clast gravels and silty clay beds occupy the lowermost slope basin deposits at Site C0008. They can be correlated as the distal parts of MTDs identified in seismic data within the lower part of unit 1c (see section 4.1 above). These lower Pleistocene deposits are time correlative to the hiatus and slide scar recognized at Site C0004. Gravel beds range from 2 to 80 cm thick and are composed of slightly indurated greenish gray to dark greenish gray, poorly sorted silty clay clasts and few pumice pebbles. The clasts range in size from <1 mm to 5 cm (Figures 10f and 11b). The matrix is olive to greenish gray silty clay or silt, and the clast-matrix fabric varies from matrix supported to clast supported. In contrast with the subangular breccia clasts, the great majority of gravel clasts are rounded to subrounded, and their 3-D shapes are generally cubic to subspherical (Figure 11). This suggests no significant postdepositional deformation or consolidation. Furthermore, there are no significant differences between clasts, matrix, and interbeds of mud in bulk density, grain density, or fractional porosity (Figure 12), which indicates that the clasts were soft at the time of deposition and that no differential compaction occurred thereafter between clasts and matrix.

[37] The only significant differences among gravel clasts, matrix, the mud interbeds, and overlying deposits of hemipelagic mud come from the composition of the clay mineral assemblages (Figure 13). All of the clast samples that we analyzed yielded lower relative percentages of chlorite + kaolinite and significantly higher contents of smectite, relative to the surrounding matrix. The consistent enrichment of smectite from matrix to

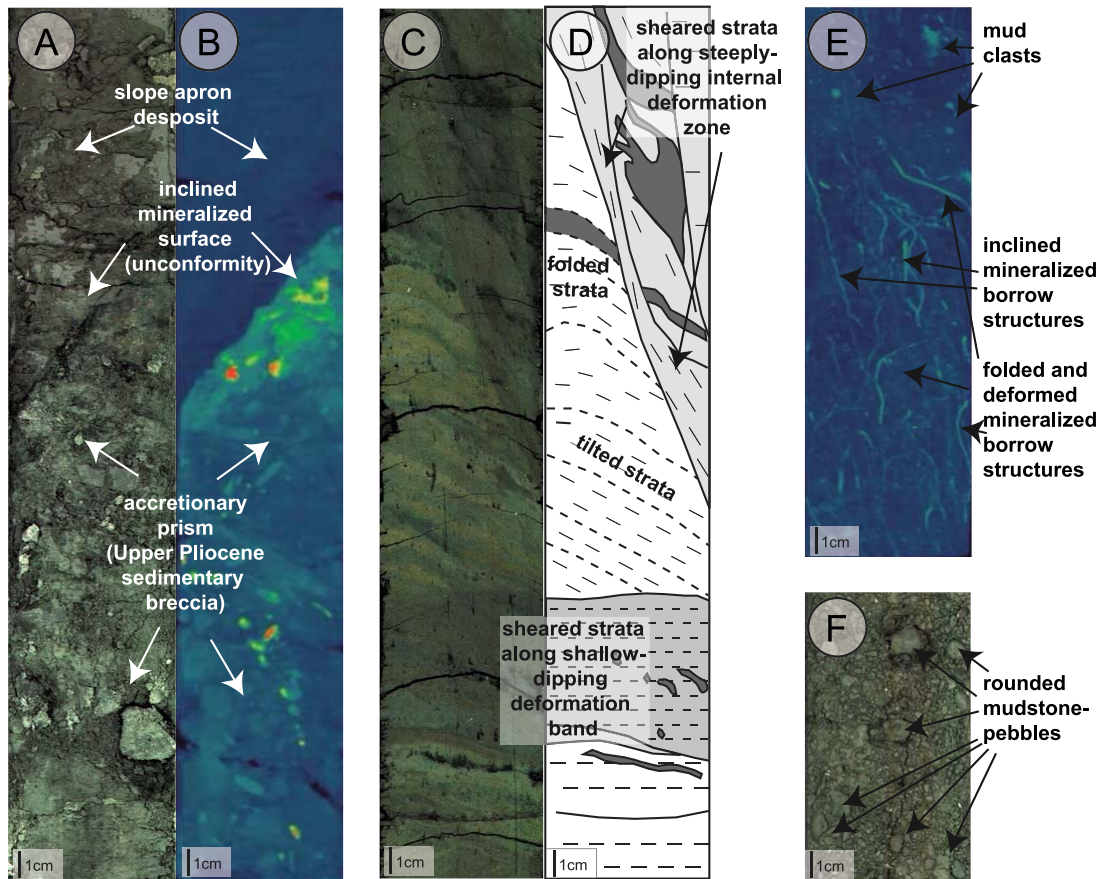


**Figure 10.** Evidence for mass movement as observed in cores and X-CT scans. (a) Visible light image of core C0004C-9H-5, 60–96 cm, showing unconformity between slope apron and accretionary prism (upper Pliocene sedimentary breccia). (b) Semitransparent rendering of X-CT image C0004C-9H-5, 60–96 cm, showing the variable density of the mineralized unconformity and underlying sedimentary breccias (3-D animation of X-CT scan provided in Animation S1). (c) Visible light image of core C0008A-2H-7, 73–110 cm, showing example of shallow slump facies in the upper part of the slope basin stratigraphic succession. (d) Interpretative sketch of slump facies in core C0008A-2H-7, 73–110 cm (Figure 10c). (e) Semitransparent rendering of X-CT image C0008C-2H-2, 0–20 cm showing slump facies identified by mud clasts overlying tilted and distorted sub-mm-scale mineralized borrow structures, which generally form as vertical cm-dm-scale subvertical tubes in undisturbed sediment (3-D animation of X-CT scan provided in Animation S2). (f) Visible light image of core C0008A-32X-1, 100–110 cm, showing rounded mudstone pebbles in MTD at the base of the slope basin stratigraphic succession.

clast averages about 10 wt %, which is well above the error of the method (<3 wt %).

[38] Previous studies of the Nankai depositional system (including sites in the Shikoku Basin) provide a robust framework to interpret these results. Those XRD data have established consistent temporal trends in the clay mineral assemblages, which have been linked to gradual changes in terrestrial sediment sources and deep-marine dispersal systems. Smectite content is the most diagnostic indicator of stratigraphic affinity because those values gradually increase downsection and show the most spread [Underwood and Pickering, 1996]. Following that logic, the most likely provenance

for mud clasts with moderate contents of smectite (~40–50 wt %) is within the upper Miocene to lower Pliocene interval of the stratigraphy [e.g., Steurer and Underwood, 2003]. This interpretation of a recycled Miocene-Pliocene prism source for the mud clasts is supported further by XRD data from Sites C0001, C0002, and C0004 [Guo *et al.*, 2009]. Although the mineral assemblages from older slope apron deposits display some overlap with younger accretionary prism samples, the MTD clasts show greater compositional affinity to an average value for early Pliocene or latest Miocene samples from the accretionary prism (Figure 13). We suggest, therefore, that accreted Pliocene strata in the hanging wall of the megasplay fault acted as

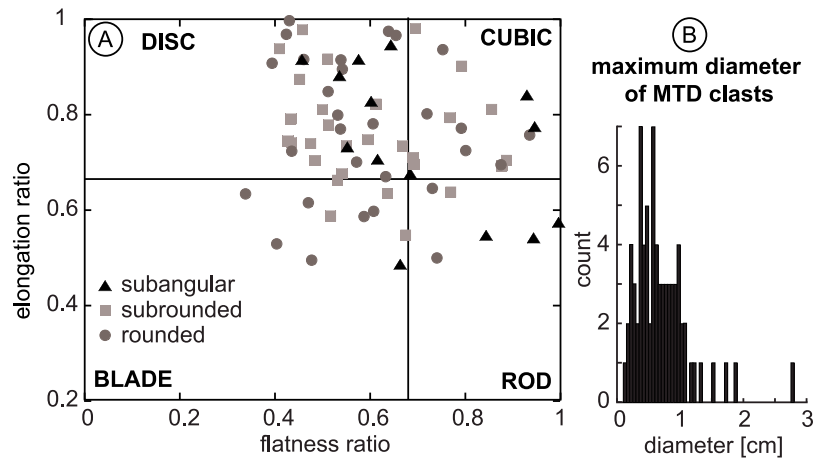


**Figure 11.** Texture of MTD clasts. (a) Zingg's diagram [Drake, 1970] showing particle shape and sphericity of 72 analyzed individual clasts sampled from MTDs recovered from the lowermost part of the slope stratigraphic succession at Sites C0008A and C, as a function of their elongation and flatness ratio. Roundness of clasts follows classification by Pettijohn *et al.* [1972]. (b) Histogram of maximum diameter of individual MTD clasts.

the primary source for mud clasts within the MTDs. Similarities among physical index properties between MTD clasts and Pliocene prism samples reinforce this compositional interpretation (Figure 12).

[39] We see ample evidence of erosion and remobilization of slightly indurated accreted material that had been thrust up along the megasplay fault, and the subsequent mass transport of mud clasts occurred while the clasts were supported by a matrix of sandy mud (i.e., as cohesive debris flows). Some of the source material may have been modified into mud clasts before remobilization (e.g., sedimentary breccias in the upper Pliocene MTD at Site C0004). This type of recycling would explain the peculiar rounded clast geometries. Hence, the brecciated slide scar at Site C0004 could be genetically linked to the upper Pleistocene MTDs at Site C0008 (see further discussion below in section 5.1).

[40] Cores from the younger slope basin deposits immediately overlying the upper Pleistocene MTDs at Site C0008 (i.e., the upper part of unit 1c and unit 1b) lack clear evidence for MTDs. However, nannofossil assemblages within this succession show mixing and reworking of older species between ~1.6 and 1.07 Ma [Expedition 316 Scientists, 2009d; Su, submitted manuscript, 2010], which might be a consequence of frequent remobilization of the slope apron.

[41] Additional evidence for MTDs are observed in the shallowest part of Site C0008, within core 2H, and is related to the stratigraphic gap ranging between ~0.9 Ma and 0.06 Ma [Expedition 316 Scientists, 2009d; Su, submitted manuscript, 2010]. Where the sediment shows color banding and interbeds of sand and silt, rotation and shearing resulted in deformed and distorted stratification (Figures 10c and 10d). Where the sediment is homogenous greenish gray silty clay, evidence for

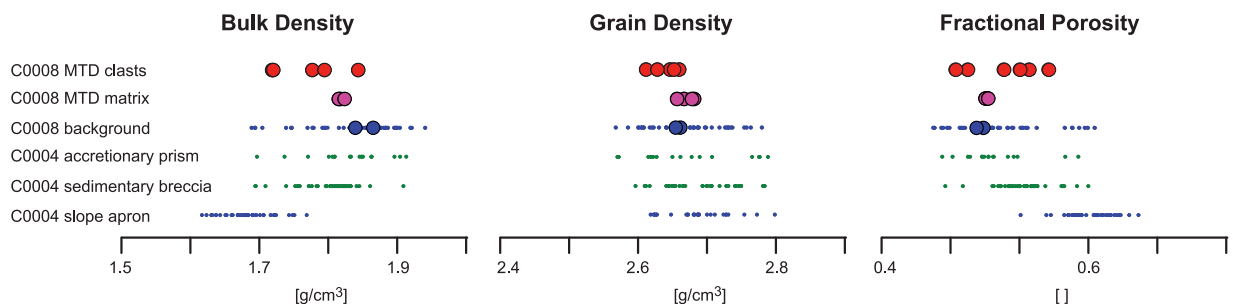


**Figure 12.** Comparison of physical index properties between MTD clasts, MTD matrix, and surrounding background sediment recovered from the lowermost part of the slope stratigraphic succession at Sites C0008A and C, and potential MTD source material (see text for discussion).

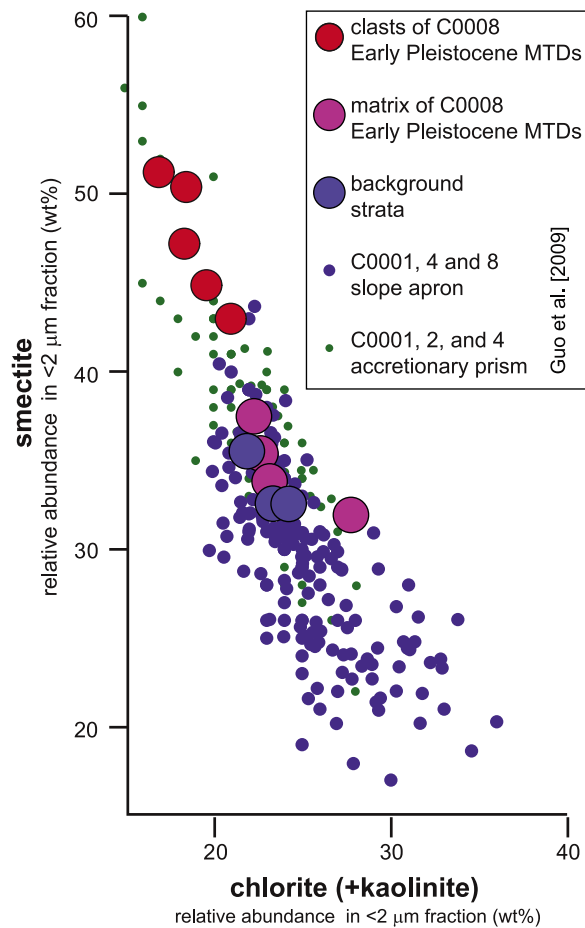


**Figure 13.** Clay mineralogy of the clay size fraction, expressed as a function of the weight percent of smectite and (chlorite+kaolinite). Significant differences exist between MTD clasts, matrix, and overlying/interbedded background strata. As a comparison, the XRD data from Sites C0001, 2, 4, and 8 [Guo *et al.*, 2009] are plotted as two broad classes distinguishing between slope apron sediment (blue dots) and older accreted strata (green dots) (see text for discussion).

sediment mass movement can only be recognized in X-CT images that show small differences in density; for example, small sub-mm-scale mineralized borrow structures, which generally form as vertical cm-dm-scale subvertical tubes in undisturbed sediment. Figure 10e (and Animation S2) shows semitransparent rendering of an X-CT image (and 3-D visualization animation, respectively) that appears homogenous upon visual examination of the split core. This image shows a chaotic organization of the mineralized borrow structures, suggesting that most of the homogenous silty clay in core C0008A-2H is a MTD. Its origin most likely relates to the slump scar described above in section 4.1. This relation is reinforced by

the fact that, near-seafloor porosity values are anomalously low, suggesting removal of overburden sediment, of estimated thickness 105 m at this site [Conin *et al.*, 2011]. This estimate is comparable by order of magnitude to our minimum estimate for erosion by slumping interpreted from seismic data (90 m; see section 4.1 above). We therefore interpret the MTD observed in core C0008A-2H as very proximal deposit of this slump, possibly also related to slope readjustment of the relatively steep head scar region after the main slope failure event.

[42] No comparable evidence for slump or debris flow deposits was observed in cores from the uppermost part of Site C0004, where biostratigraphy and paleomagnetic data document the absence of sediment younger than 0.44 Ma. At this site, Conin *et al.* [2011] also report anomalously low porosity near the seafloor and suggest that this age gap is best explained by recent erosion of ~57 m of overburden. This interpretation is further supported by geometric manifestations of slump scars in seismic and bathymetric data, from which we estimate a minimum value for recent erosion by slumping of ~40 m (see above in section 4.1). Only a thin veneer of sediment, which is at least ~10,000 years old, was deposited after the erosional event, as indicated by radiocarbon stratigraphy of the top meter at Site C0004 (A. Sakaguchi *et al.*, Episodic seafloor mud brecciation due to great subduction zone earthquakes, submitted to *Geology*, 2011). This interval also comprises the youngest evidence for sediment mobilization and redeposition in the study area, with repeated occurrences of few cm thick mud breccias, the youngest of which has been deposited within the last 40–60 years (Sakaguchi *et al.*, submitted manuscript, 2011). They suggest that this youngest example of seafloor mud brecciation correlates to the most recent megathrust earthquake in the study area, the  $M_w$  8.2 Tonankai earthquake in 1944 [Ando, 1975].

## 5. Discussion

[43] Core and seismic data presented above document various mass movements of different scales that have affected the accreted strata that were thrust up along the megasplay fault and slope sediments, above and seaward of the MSFZ. The mass movement features range in age from 2.87 Ma to very recent (within the last century). This time period spans the system's tectonostratigraphic evolution from frontal accretion in a prism toe position, to an emergence of trench slope basin

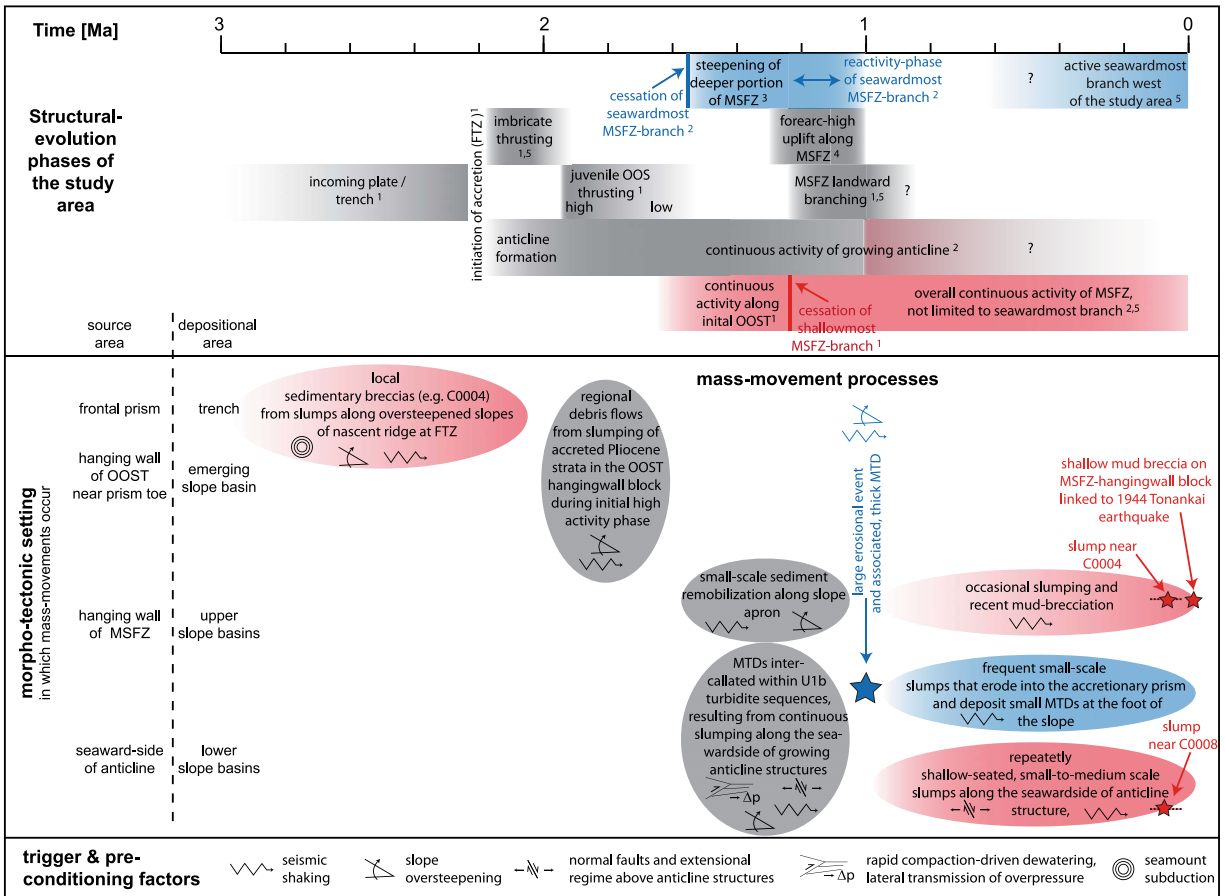


**Figure 14.** Schematic summary representation showing timing, nature, and inferred trigger mechanisms and preconditioning factors for submarine mass movement processes observed in the study area in relation to their morphotectonic setting in which they occur and the tectonic evolution of the Nankai fore arc. The colors indicate whether processes affected the whole study area (gray) or only the western and eastern domain (blue and red, respectively). The structural evolution phases are summarized after (1) *Strasser et al.* [2009], (2) *Kimura et al.* [2011], (3) *Bangs et al.* [2009], (4) *Gulick et al.* [2010], and (5) *Moore et al.* [2007]. FTZ, frontal thrust zone; OOST, out-of-sequence thrust; MSFZ, megasplay fault zone; MTD, mass transport deposit. Blue and red stars indicated individual slump events described in detail in this study, and colors indicated the area in which they occurred (western and eastern part of the study area, respectively). See section 5 for detailed discussion.

sedimentation and out-of-sequence thrusting, to uplift, ongoing megasplay activity and late Pleistocene to Holocene slope apron sediment deposition [Strasser et al., 2009]. Hence, submarine slope failure scars and MTDs in different stratigraphic positions reflect processes within different morphotectonic regimes of the evolving Nankai margin. In sections 5.1–5.4, we place the observed mass movement features into a context of how tectonostratigraphic position might have influenced their mechanical behavior. A schematic summary is presented in Figure 14, which shows the timing and setting of mass-wasting events and processes in relation to the tectonic evolution of the area.

### 5.1. Slope Failure at the Deformation Front and Along the Juvenile Splay Fault System

[44] The structure, fabric, age, and stratigraphic position of the upper Pliocene MTD cored at Site C0004C collectively indicate that it formed by episodic remobilization of strata at shallow burial depths near the toe of the late Pliocene accretionary prism. Due to its limited lateral extent, we interpret this MTD as a local phenomenon and, thus, it may have been nothing more than a small slump along the oversteepened slope of a nascent ridge at the deformation front. The products of comparable processes are observed in bathymetric data of the modern prism toe environment. Frontal collapses of

different sizes and scales create embayment structures and hummocky deposits that deflect the trench's axial channel to a more seaward position [Kawamura *et al.*, 2010]. A long-lasting deflection or complete blockage of axial transport systems may also help to explain why the uppermost part of accretionary prism is anomalously mudstone rich at Sites C0001 and C0004 [Expedition 315 Scientists, 2009a; Expedition 316 Scientists, 2009c]. Frontal oversteepening and collapses of the prism toe are often linked to subduction of elevated seafloor topography, such as seamounts [e.g., von Huene, 2008; Screaton *et al.*, 2009].

[45] As the prism continued to evolve, and out-of-sequence thrusting initiated about 1.95 Ma, the accreted strata and late Pliocene MTD were uplifted along the juvenile splay fault, which overrode the emerging trench wedge basin [Strasser *et al.*, 2009]. At the location of Site C0004, this overthrusting resulted in a shift from a regime of sediment accumulation to a location on the steepening hanging wall, along which slope failure and remobilization of poorly consolidated material predominated. This adjustment is preserved in the stratigraphy by the buried slide scar at Hole C0004C, and the erosional products that were deposited between ~1.95 and 1.8 Ma in the adjacent slope basin. This period of slope failures and MTD formation is time correlative to a high-activity phase of fault movements along the splay fault, as documented by >1300 m of horizontal throw in only 150 ka (8.6 m/ka) [Strasser *et al.*, 2009]. Likewise, onset of sedimentation above the slide scar, and cessation of mass transport deposition in the slope basin after ~1.7 Ma, both correlate in time with a significant reduction of throw rates along the splay fault [Strasser *et al.*, 2009]. This provides strong evidence for linking fault activity to submarine mass movement initiation.

[46] Possible causal links between faults and slope failure initiation include oversteepening of slopes above the fault and dynamic loading by earthquake shaking. In particular, amplification of seismic ground shaking can occur in the hanging wall of a splay fault (hanging wall effect [Abrahamson and Somerville, 1996]) if the fault ruptures coseismically, as has been interpreted for the Nankai megasplay and other splay fault systems [e.g., Plafker, 1972; Tanioka and Satake, 2001; Baba *et al.*, 2006]. Assuming that the ~1300 m throw along the fault between 1.95 and 1.8 Ma accumulated periodically during megathrust earthquakes, and assuming meter-scale coseismic slip [Tanioka

and Satake, 2001; Kikuchi *et al.*, 2003], the long-term displacement rate would be consistent with an average earthquake recurrence interval of ~115 years, which is roughly the same as the historical record of great earthquakes across the Nankai margin [Ando, 1975].

## 5.2. Slope Failure Along the Seaward Side of Growing Anticline Structures

[47] Stacked MTDs within interbedded turbidites and mud of varying thickness cover large parts of the sedimentary succession in the lower slope basin (unit 1b). These deposits are time correlative to significant erosion occurring along the seaward dipping, low-angle surface above the growing anticline that separates the upper from the lower slope basin. This conclusion is supported by truncation of the high-amplitude reflections correlating to stacked turbidite deposits of unit 1b in the upper basin. As outlined above, we interpret the low-angle surface as a multiple-slump detachment surface. Sediment remobilization along this surface may partly have been by continuous small-scale slumping (Figure S2), and interpreted MTDs within the turbidite sequence in the lower basin likely represent the correlative deposits. This connection indicates yet another seaward shift of MTD source and deposition away from the MSFZ, and it likely relates to a temporal change in the deformation style of the splay fault system and the growing anticline structure within the underlying accretionary prism [Bangs *et al.*, 2009; Gulick *et al.*, 2010; Kimura *et al.*, 2011] (see section 2.2 above).

[48] The geometric relation between the low-angle surface and inferred source area of the MTD, above and seaward of the growing anticline structure, respectively, suggests that the likelihood of slope failure may be exacerbated by the extensional stress field near the top of the anticline, which also is inferred from high-angle normal faults observed in core and seismic data [Kimura *et al.*, 2011] (see also Figures 4 and 5). Another collateral contribution to instability may be the underthrusting of highly permeable sand layers below the splay fault. Porosities are lower in the underthrust section at Site C0004 as compared to the reference section at Site C0008 [Expedition 316 Scientists, 2009c, 2009d] (see section 2.3 above). Compaction-induced dewatering of mud during underthrusting was very efficient, likely by draining into interbeds of sand and lateral fluid flow [Kimura *et al.*, 2008]. In addition to pressure transmission within the

slope basin sediments, the sand-rich interval that forms the anticline beneath the megasplay may also transmit fluid pressure [Rowe and Screaton, 2009]. Where these permeable layers meet low overburden on steepening slopes of the growing anticline structures, fluid overpressures and lower effective stress may have reduced the shear strength enough to promote frequent failure. Lateral transmission of overpressured fluids from areas with thicker to thinner overburden is a mechanism for enhancing slope failure along passive continental margins [Dugan and Flemings, 2000]. In subduction zones, comparable conditions might exist where out-of-sequence faults override slope basins. Additionally, transient pulses of high pore pressure may be transferred along sand beds during megathrust earthquakes. Seismic ground shaking also enhances the chances of submarine slope failure.

### 5.3. Large-Scale Slope Collapse Along the SW Hanging Wall Block of the Megasplay Fault

[49] At about 1 Ma an exceptional mass-wasting event eroded a large part of the upper slope basin, slope apron, and hanging wall of the MSFZ in the SW part of the study area. This led to deposition of a prominent, up to 182 m thick MTD in the lower slope basin. On the basis of the geometric relation between the splay fault and slope failure scar (see section 4.1 above and Figure 8), we speculate that slope failure may have been triggered by movement along the splay and/or by fluid expulsion along the fault into the bedding-parallel basal glide plane of the slide. This interpretation is supported by the temporal coincidence of the megacollapse with a period of extensive motion along the megasplay between 1.3 and 1 Ma [Gulick *et al.*, 2010]. Bangs *et al.* [2009] documented steepening of the splay fault in the western portion from asymmetric fore-arc high uplift and thickness distribution of a large volume of underthrust sediment beneath the thrust. This interval of accretion likely resulted in slope oversteepening and an unfavorable shift toward lower slope stability, preconditioning the slope to failure.

### 5.4. Younger Slumps Affecting the Eroded Prism and the Upper Sedimentary Cover

[50] As outlined above in section 4.1, the exceptionally thick MTD separates the stratigraphic succession of the lower slope basin into two parts, thereby recording a change in the style of deposition and mass movement around that time. Direct

influence of splay fault activity was likely reduced, as we see no direct evidence for displacement along the seaward most branch of the splay fault younger than ~1.24–1 Ma. If the effects of differential compaction and lateral transmission of fluids were reduced as a consequence (possibly also in line with a general decrease in sedimentation rates with cessation of turbidite deposition), this may explain why younger MTDs in the study area are smaller than its older counterpart.

[51] We also document significant along-strike variations in the upper slope basin and MSFZ slope area (see section 4.1 above). We attribute these variations to the legacy of the large slope collapse that occurred around ~1 Ma. That event significantly changed the slope geometry and eroded most of the upper slope cover. Additionally, the differences may relate to a structural separation between the eastern and western portion of the MSFZ as reported by Kimura *et al.* [2011]. Frequent mass wasting and synsedimentary deformation in the eastern part may be related to the fact that deformation there is much broader and scattered, as well as interrelated with deformation of the underlying accretionary prism and not limited to the splay fault only. The preconditioning scenarios for shallow-seated slides confined to the sedimentary cover, therefore, may be similar to our description above. The contribution from ground accelerations during large earthquakes, and related transient pore pressure phenomena, then constitute a plausible trigger mechanism for sediment instability. This idea is supported by core-derived evidence for the most recent mobilization and redeposition of sediment; a thin mud brecciation layer related to the 1944  $M_w$  8.2 Tonankai earthquake (Sakaguchi *et al.*, submitted manuscript, 2011).

## 6. Summary and Conclusions

[52] IODP cores and 3-D reflection seismic data from the shallow MSFZ and adjacent slope basin of the Nankai accretionary wedge record a history of multifarious submarine mass movements spanning from 2.87 Ma to within the last century. We document how downslope sediment mass transfer and sediment redistribution influenced the stratigraphic evolution of the slope system overlying folds and thrusts in the evolving Nankai accretionary wedge. The scale and styles of submarine slope failures changed temporally and spatially, and those changes were closely linked to the morphotectonic setting in which the mass movements occurred

(Figure 14). Of paramount importance for the stratigraphic evolution and mass transport deposition were the activity and style of deformation along the megasplay fault, as was formation of anticlinal structures in the underlying accretionary prism. Periods of increased slumping and mass flow deposition coincided with pulses of enhanced structural activity. This linkage can be documented for three noteworthy episodes: (1) the 1.95–1.7 Ma MTDs that were fed by slope failures along the evolving hanging wall of the MSFZ during an initial high-activity phase of the juvenile out-of-sequence thrust system, (2) slope failures between ~1.55 and 1.24 Ma along the seaward side of growing anticline structures (during this time period a stratigraphic interval with abundant sand beds was thrust beneath the megasplay, and the combination of rapid compaction-driven dewatering and lateral transmission of overpressured fluids may have lowered effective stress enough to precondition the slopes for frequent failure), and (3) the prominent landslide event around 1 Ma, which may have been triggered by movement along the splay fault and/or by fluid expulsion along the fault into the basal glide plane during a period of enhanced megasplay activity.

[53] We conclude that the structural evolution of imbricated thrusts and the MSFZ, with their punctuated episodes of tectonic activity, is what exerted the key influences over magnitude and frequency of submarine slides in the Nankai fore arc. This has important implications for comparable settings of other convergent margins. The tectonics of subduction-accretion affects slope geometry and stress regime in the hanging wall of out-of-sequence thrusts, as well as near the top of anticlinal structures within the accretionary prism. Additionally, the growth of anticlines with highly permeable sand layers, together with overthrusting of sandy slope basins by out-of-sequence thrusts, probably sets up hydrologic conditions in which differential compaction and lateral transmission of overpressured fluids leads to localized reductions of effective stress. Hence, the tectonic regime sets up preconditions to exacerbate the chances of submarine slope failure. In addition, megathrust earthquakes probably contribute to slope failure through dynamic loading by seismic waves and/or further reductions of shear strength from transient pulses of high pore pressure. Our study further demonstrates that detailed knowledge about the spatial and temporal distribution of MTDs in accretionary prism slope basin environments, along with an understanding of their underlying physical

origins, can be integrated into a holistic reconstruction of the tectonostratigraphic evolution of subduction margins.

## Acknowledgments

[54] This research used samples and data provided by the Integrated Ocean Drilling Program (IODP). The authors thank the sedimentology, biostratigraphy and magnetostratigraphy groups of Expedition 316 (C. Fergusson, F. Girault, Y. Kitamura, K. Milliken, U. Nicholson, A. Sakaguchi, X. Su, and X. Zhao) and *Paradigm Geophysical* for providing the seismic interpretation software used in this study. The Associate Editor and a reviewer are acknowledged for providing constructive comments that helped to improve this paper. This work was supported by grants from the DFG-Research Centre/Cluster of Excellence MARUM-“The Ocean in the Earth System” (to M.S. and A.K.), the European Science Foundation (ESF) “Workshop on Marine Research Drilling (Magellan Workshop Series)” (to M.S.), the U.S. National Science Foundation to the University of Hawaii, U.S.A (OCE-0451790), to the University of Florida (OCE-0727023), and to the University of Missouri (OCE-07518190), and the Consortium for Ocean Leadership (to M.U and J.G.; grants T315B58 and T315C58).

## References

- Abrahamson, N. A., and P. G. Somerville (1996), Effects of the hanging wall and footwall on ground motions recorded during the Northridge earthquake, *Bull. Seismol. Soc. Am.*, *86*, S93–S99.
- Ando, M. (1975), Source mechanisms and tectonic significance of historical earthquakes along the Nankai Trough, Japan, *Tectonophysics*, *27*, 119–140, doi:10.1016/0040-1951(75)90102-X.
- Ashi, J., and A. Taira (1992), Structure of the Nankai accretionary prism as revealed from IZANAGI sidescan imagery and multichannel seismic reflection profiling, *Isl. Arc, J.*, 104–115, doi:10.1111/j.1440-1738.1992.tb00063.x.
- Baba, T., et al. (2006), High precision slip distribution of the 1944 Tonankai earthquake inferred from tsunami waveforms: Possible slip on a splay fault, *Tectonophysics*, *426*, 119–134, doi:10.1016/j.tecto.2006.02.015.
- Bangs, N. L. B., et al. (2009), Broad, weak regions of the Nankai Megathrust and implications for shallow coseismic slip, *Earth Planet. Sci. Lett.*, *284*, 44–49, doi:10.1016/j.epsl.2009.04.026.
- Blum, P. (1997), Physical properties handbook: A guide to the shipboard measurement of physical properties of deep-sea cores, *Tech. Note 26*, Ocean Drill. Program, College Station, Tex. [Available at <http://www-odp.tamu.edu/publications/tnotes/tn26/INDEX.HTM>.]
- Burg, J. P., et al. (2008), A giant catastrophic mud-and-debris flow in the Miocene Makran, *Terra Nova*, *20*, 188–193, doi:10.1111/j.1365-3121.2008.00804.x.
- Camerlenghi, A., and G. A. Pini (2009), Mud volcanoes, olistostromes and Argille scagliose in the Mediterranean region, *Sedimentology*, *56*, 319–365, doi:10.1111/j.1365-3091.2008.01016.x.



- Camerlenghi, A., et al. (2007), Scientific Ocean Drilling Behind the Assessment of geo-hazards from submarine slides, *Sci. Drill.*, 4, 45–47, doi:10.2204/iodp.sd.4.14.2007.
- Chaytor, J. D., et al. (2009), Size distribution of submarine landslides along the U.S. Atlantic margin, *Mar. Geol.*, 264, 16–27, doi:10.1016/j.margeo.2008.08.007.
- Cochonat, P., et al. (2002), Slope instabilities and gravity processes in fluid migration and tectonically active environment in the eastern Nankai accretionary wedge (KAIKO-Tokai'96 cruise), *Mar. Geol.*, 187, 193–202, doi:10.1016/S0025-3227(02)00266-9.
- Conin, M., et al. (2011), Interpretation of LWD resistivity from Nankai accretionary wedge in the light of clay physico-chemical properties: Evidence for erosion and local overpressuring, *Geochem. Geophys. Geosyst.*, Q0AD07, doi:10.1029/2010GC003381.
- Drake, L. D. (1970), Rock texture; an important factor for clast shape studies, *J. Sediment. Petrol.*, 40, 1356–1361.
- Dugan, B., and P. B. Flemings (2000) Overpressure and fluid flow in the New Jersey continental slope: Implications for slope failure and cold seeps, *Science*, 289, 288–291.
- Expedition 315 Scientists (2009a), Expedition 315 Site C0001, in *NanTroSEIZE Stage 1: Investigations of Seismogenesis, Nankai Trough, Japan, Proc. Integr. Ocean Drill. Program*, 314/315/316, doi:10.2204/iodp.proc.314315316.123.2009.
- Expedition 316 Scientists (2009b), Expedition 316 methods, in *NanTroSEIZE Stage 1: Investigations of Seismogenesis, Nankai Trough, Japan, Proc. Integr. Ocean Drill. Program*, 314/315/316, doi:10.2204/iodp.proc.314315316.132.2009.
- Expedition 316 Scientists (2009c), Expedition 316 Site C0004, in *NanTroSEIZE Stage 1: Investigations of Seismogenesis, Nankai Trough, Japan, Proc. Integr. Ocean Drill. Program*, 314/315/316, doi:10.2204/iodp.proc.314315316.133.2009.
- Expedition 316 Scientists (2009d), Expedition 316 Site C0008, in *NanTroSEIZE Stage 1: Investigations of Seismogenesis, Nankai Trough, Japan, Proc. Integr. Ocean Drill. Program*, 314/315/316, doi:10.2204/iodp.proc.314315316.136.2009.
- Goldfinger, C., et al. (2000), Super-scale failure of the southern Oregon Cascadia margin, *Pure Appl. Geophys.*, 157, 1189–1226, doi:10.1007/s000240050023.
- Gulick, P. S., et al. (2010), Rapid forearc basin uplift and megasplay fault development from 3D seismic images of Nankai Margin off Kii Peninsula, Japan, *Earth Planet. Sci. Lett.*, 300, 55–62, doi:10.1016/j.epsl.2010.09.034.
- Guo, J., M. Underwood, D. Hillix, H. Wu, H. Banno, and U. Shrinivar (2009), Clay mineral assemblages from Nankai Trough and Kumano Basin, IODP Expeditions 315 and 316, NanTroSEIZE Stage 1, *Eos Trans. AGU*, 90(52), Fall Meet. Suppl., Abstract T21C-1840.
- Hampton, M. A., et al. (1996), Submarine landslides, *Rev. Geophys.*, 34, 33–59, doi:10.1029/95RG03287.
- Henry, P., et al. (2002), Surface expression of fluid venting at the toe of the Nankai wedge and implications for flow paths, *Mar. Geol.*, 187, 119–143, doi:10.1016/S0025-3227(02)00262-1.
- Hühnerbach, V., and D. G. Masson (2004), Landslides in the North Atlantic and its adjacent seas: An analysis of their morphology, setting and behavior, *Mar. Geol.*, 213, 343–362, doi:10.1016/j.margeo.2004.10.013.
- Hühnerbach, V., et al. (2005), Deformation and submarine landsliding caused by seamount subduction beneath the Costa Rica continental margin—new insights from high-resolution sidescan sonar data, in *Submarine Slope Systems: Processes and Products*, edited by D. M. Hodgson and S. S. Flint, *Geol. Soc. Spec. Publ.*, 244, 195–205, doi:10.1144/GSL.SP.2005.244.01.12.
- Kawamura, K., et al. (2009), Structural architecture and active deformation of the Nankai Accretionary Prism, Japan: Submersible survey results from the Tenryu Submarine Canyon, *Geol. Soc. Am. Bull.*, 121, 1629–1646, doi:10.1130/B26219.1.
- Kawamura, K., et al. (2010), Redistribution of Sediments by Submarine Landslides on the Eastern Nankai Accretionary Prism, in *Submarine Mass Movements and Their Consequences*, edited by D. C. Mosher et al., pp. 313–322, Springer, Dordrecht, Netherlands, doi:10.1007/978-90-481-3071-9\_26.
- Keefe, D. K. (1984), Landslides caused by earthquakes, *Geol. Soc. Am. Bull.*, 95, 406–421, doi:10.1130/0016-7606(1984)95<406:LCBE>2.0.CO;2.
- Kikuchi, M., et al. (2003), Source rupture processes of the 1944 Tonankai earthquake and the 1945 Mikawa earthquake derived from low-gain seismograms, *Earth Planets Space*, 55, 159–172.
- Kimura, G., E. J. Screaton, D. Curewitz, and Expedition 316 Scientists (2008), NanTroSEIZE Stage 1A: NanTroSEIZE shallow megasplay and frontal thrusts, *Integr. Ocean Drill. Program Prelim. Rep.*, 316, doi:10.224/iodp.pr.316.2008.
- Kimura, G., et al. (2011), Spatial and temporal evolution of the megasplay fault in the Nankai Trough, *Geochem. Geophys. Geosyst.*, 12, Q0A008, doi:10.1029/2010GC003335.
- Kinoshita, M., H. Tobin, J. Ashi, G. Kimura, S. Lallemand, E. J. Screaton, D. Curewitz, H. Masago, K. T. Moe, and the Expedition 314/315/316 Scientists (2009), *Proceedings of the Integrated Drilling Program Expeditions*, vol. 314/315/316, Integr. Ocean Drill. Program, Washington, D. C., doi:10.2204/iodp.proc.314315316.2009.
- Lee, H. J., et al. (2007), Submarine mass movements on continental margins, in *Continental Margin Sedimentation: From Sediment Transport to Sequence Stratigraphy*, edited by C. A. Nittrouer et al., pp. 213–273, Blackwell, Oxford, U. K.
- Locat, J., and H. J. Lee (2002), Submarine landslides: Advances and challenges, *Can. Geotech. J.*, 39, 193–212, doi:10.1139/t01-089.
- Lucente, C. C., and G. A. Pini (2008), Basin-wide mass-wasting complexes as markers of the Oligo-Miocene foredeep-accretionary wedge evolution in the Northern Apennines, Italy, *Basin Res.*, 20, 49–71, doi:10.1111/j.1365-2117.2007.00344.x.
- Martin, K. M., et al. (2010), Possible strain partitioning structure between the Kumano fore-arc basin and the slope of the Nankai Trough accretionary prism, *Geochem. Geophys. Geosyst.*, 11, Q0AD02, doi:10.1029/2009GC002668.
- Martin, V., et al. (2004), Erosion and sedimentation as processes controlling the BSR-derived heat flow on the Eastern Nankai margin, *Earth Planet. Sci. Lett.*, 222, 131–144, doi:10.1016/j.epsl.2004.02.020.
- Masson, D. G., et al. (2006), Submarine landslides: Processes, triggers and hazard prediction, *Philos. Trans. R. Soc. A*, 364, 2009–2039, doi:10.1098/rsta.2006.1810.
- McAdoo, B. G., et al. (2004), Seafloor geomorphology of convergent margins: Implications for Cascadia seismic hazard, *Tectonics*, 23, TC6008, doi:10.1029/2003TC001570.
- Moore, D. G., et al. (1976), Large submarine slide (olistostrome) associated with Sunda Arc subduction zone, northeast Indian Ocean, *Mar. Geol.*, 21, 211–226, doi:10.1016/0025-3227(76)90060-8.



- Moore, G. F., et al. (2007), Three-dimensional splay fault geometry and implications for tsunami generation, *Science*, 318, 1128–1131, doi:10.1126/science.1147195.
- Moore, G. F., et al. (2009), Structural and seismic stratigraphic framework of the NanTroSEIZE Stage 1 transect, in *NanTroSEIZE Stage 1: Investigations of Seismogenesis, Nankai Trough, Japan, Proc. Integr. Ocean Drill. Program*, 314/315/316, doi:10.2204/iodp.proc.314315316.102.2009.
- Moore, J. G., et al. (1994), Giant Hawaiian landslides, *Annu. Rev. Earth Planet. Sci.*, 22, 119–144, doi:10.1146/annurev.ea.22.050194.001003.
- Morgan, J. K., et al. (2008), Addressing geohazards through ocean drilling, *Sci. Drill.*, 7, 15–30, doi:10.2204/iodp.sd.7.01.2009.
- Morley, C. K. (2009), Growth of folds in a deep-water setting, *Geosphere*, 5, 59–89, doi:10.1130/GES00186.1.
- Mosher, D. C., et al. (2008), Deformation of the northern Sumatra accretionary prism from high-resolution seismic reflection profiles and ROV observations, *Mar. Geol.*, 252, 89–99, doi:10.1016/j.margeo.2008.03.014.
- Mosher, D. C., et al. (Eds.) (2010), *Submarine Mass Movements and Their Consequences*, 786 pp., Springer, Dordrecht, Netherlands, doi:10.1007/978-90-481-3071-9.
- Park, J. O., et al. (2002), Splay fault branching along the Nankai subduction zone, *Science*, 297, 1157–1160, doi:10.1126/science.1074111.
- Pettijohn, F. J., et al. (1972), *Sand and Sandstones*, 618 pp., Springer, New York.
- Plafker, G. (1972), Alaskan Earthquake of 1964 and Chilean Earthquake of 1960: Implications for arc tectonics, *J. Geophys. Res.*, 77, 901–925, doi:10.1029/JB077i005p00901.
- Rowe, K. T., and E. J. Screaton (2009), Permeabilities of core samples from Integrated Ocean Drilling Program Expedition 316 and implications for shallow fluid flow due to megasplay fault movement, *Eos Trans. AGU*, 90(52), Fall Meet. Suppl., Abstract T21C-1839.
- Screaton, E., et al. (2009), Interactions between deformation and fluids in the frontal thrust region of the NanTroSEIZE transect offshore the Kii Peninsula, Japan: Results from IODP Expedition 316 Sites C0006 and C0007, *Geochem. Geophys. Geosyst.*, 10, Q0AD01, doi:10.1029/2009GC002713.
- Smit, J., et al. (2010), Effects of mass waste events on thrust wedges: Analogue experiments and application to the Makran accretionary wedge, *Tectonics*, 29, TC3003, doi:10.1029/2009TC002526.
- Steurer, J. F., and M. B. Underwood (2003) Clay mineralogy of mudstones from the Nankai Trough reference Sites 1173 and 1177 and frontal accretionary prism Site 1174, *Proc. Ocean Drill. Program Sci. Results*, 190/196 [online]. [Available at <http://www-odp.tamu.edu/publications/190196SR/211/211.htm>.]
- Strasser, M., et al. (2009), Origin and evolution of a splay fault in the Nankai accretionary check, *Nat. Geosci.*, 2, 648–652, doi:10.1038/ngeo609.
- Taira, A., et al. (2005), Nankai Trough Seismogenic Zone Site Survey: Kumano Basin Seismic Survey, *CDEX Tech. Rept.*, vol. 1, 64 pp., Jpn. Agency for Mar.-Earth Sci. and Technol., Yokohama, Japan.
- Tanioka, Y., and K. Satake (2001), Detailed coseismic slip distribution of the 1944 Tonankai earthquake estimated from tsunami waveforms, *Geophys. Res. Lett.*, 28, 1075–1078, doi:10.1029/2000GL012284.
- Tobin, H. J., and M. Kinoshita (2006), NanTroSEIZE: The IDOP Nankai Trough seismogenic zone experiment, *Sci. Drill.*, 2, 23–27.
- Underwood, M. B., and K. T. Pickering (1996), Clay-mineral provenance, sediment dispersal patterns, and mudrock diagenesis in the Nankai accretionary prism, southwest Japan, *Clays Clay Miner.*, 44, 339–356, doi:10.1346/CCMN.1996.0440304.
- Underwood, M., N. Basu, J. Steurer, and S. Udas (2003a) Data report: Normalization factors for semiquantitative X-ray diffraction analysis, with application to DSDP Site 297, Shikoku Basin, *Proc. Ocean Drill. Program Sci. Results*, 190/196 [online]. [Available at <http://www-odp.tamu.edu/publications/190196SR/203/203.htm>.]
- Underwood, M. B., et al. (2003b), Sedimentary and tectonic evolution of a trench-slope basin in the Nankai subduction zone of southwest Japan, *J. Sediment. Res.*, 73, 589–602, doi:10.1306/092002730589.
- von Huene, R. (2008), When seamounts subduct, *Science*, 321, 1165–1166, doi:10.1126/science.1162868.
- von Huene, R., C. R. Ranero, and P. Watts (2004), Tsunami-genic slope failure along the Middle America Trench in two tectonic settings, *Mar. Geol.*, 203, 303–317, doi:10.1016/S0025-3227(03)00312-8.
- Yamada, Y., et al. (2010), Submarine landslides at subduction margins: Insights from physical models, *Tectonophysics*, 484, 156–167, doi:10.1016/j.tecto.2009.09.007.